Dynamics and synchronization of two and three delay-coupled semiconductor lasers

Tesis presentada por
M. en C. Diana Alejandra Arroyo Almanza

Asesor
Alexander N. Pisarchik

Como requisito para obtener el grado de
Doctor en ciencias (Óptica)

Versión Final, como requisito para presentar el examen Doctoral

León, Gto. 30 de Mayo de 2013

Acknowledgments

First of all I would like to thank Dr. Alexander N. Pisarchik for his guidance throughout the development of this thesis. I learned a lot working with him and he was able to transmit me his enthusiasm in this field of physics.

I would also like to thank Dr. Claudio Mirasso, Dr. Miguel Cornelles, and Dr. Ingo Fisher for giving me the opportunity to work with them and their wise advice during the international exchange program held at the Institute for Cross-Disciplinary Physics and Complex Systems (IFISC) of Balearic University in Mallorca, Spain during four months.

In the same vein, I want to expresses my gratitude to Dr. Vacile Z. Tronciu for his wise advice during the international exchange program held at the Weierstrass Institute for Applied Analysis and Stochastic (WIAS) in Berlin, Germany. (30/May/2011 to 3/June/2011).

I would also express my gratitude to the Consejo Nacional de Ciencia y Tecnología (CONACYT) for the financial support through project No. 100429 and for the scholarship of CONACYT 1123.

Summary

The interest in a study of the dynamics of coupled semiconductor lasers results from their unique features, such as high gain, low facet reflectivity and very high sensitivity to optical injection. The diversity of temporal and optical spectral regimes is beneficial for the application of these lasers in optical communications that use the laser output as a chaotic carrier. In this thesis, we study the dynamics and synchronization of chaotic semiconductor lasers coupled in two different configurations.

The first part of the thesis is devoted to the experimental study of the dynamical behavior and synchronization of two identical (or almost identical) mutually delay-coupled semiconductor lasers, with respect to two control parameters, namely, the laser bias current and the coupling strength. Our motivation to conduct this study is the availability of a new generation of instruments, such as high-resolution optical analyzers and high-speed real-time digital oscilloscopes that enable the characterization of the dynamical properties of delay-coupled semiconductor lasers with unprecedented precision. The time series, frequency (rf) and optical spectra analyses allowed us to reveal the transition from stable continuous-wave (CW) emission of the uncoupled lasers to the regime of low frequency fluctuations (LFF) when the coupling strength is increased. In the second part, we consider a ring of three unidirectionally coupled semiconductor lasers that is an elementary cell of a complex laser network. This research allows us to know what route to chaos the ring of lasers will exhibit while the coupling strength is increasing, and how the lasers will be synchronized on this route. While uncoupled, the lasers stay within a CW regime, but when the coupling strength reaches a certain threshold value, they begin to oscillate. As the coupling further increases, the dynamics exhibit a route to chaos via a sequence of Hopf bifurcations that result in periodic, quasiperiodic and chaotic oscillations. In the chaotic range, different synchronization states, ranging from asynchronous behavior to phase and near synchronization, are observed. The analytical solution yields a large number of fixed points.

Contents

Nomenclature

Simbol	Name	Units
α	Linewidth enhancement factor	Adimensional
E	Normalized electric field normalized	Adimensional
E_x	Real part of electric field normalized	Adimensional
E_y	Imaginary part of electric field	Adimensional
h	Planck's constant	eV·s
υ	Frequency of the photon	Hz
K	Momentum	kg·m/s
λ	Wavelength	m
L	Cavity length of semiconductor laser	m
c	Speed of light in vacuum	m/s
N	Normalized carrier density normalized	Adimensional
ω	Angular frequency	rad/s
n	Real part of the refractive index	Adimensional
n''	Imaginary part of the refractive index	Adimensional
α_{abs}	Power absorption coefficient	m^{-1}
R	Reflectivity if the mirror	Adimensional
α_s	Internal loss factor	m^{-1}
$\omega_{th,m}$	Lasing frequency	rad/s
P_{pol}	Macroscopic polarization	C/m^2
ε_0	Vacuum permittivity coefficient	$F \cdot m^{-1}$
G_n	Optical gain	m^{-1}
e	electric charge	C
τ_n	Carrier lifetime	s

τ_p	Photon lifetime	s
τ	Round trip time of light	s
I_{th}	Solitary laser threshold injection current	A
I	Injection current	A
k	Coupling strength	s^{-1}
τ_c	Coupling time	s
L	Fiber length of the coupling path	m
f_0	Central frequency of the emission of laser	Hz
C_{max}	Cross correlation coefficient	Adimensional

Chapter 1. Introduction

"Something as small as the flutter of a butterfly can cause a hurricane somewhere in the world."

Edward Norton Lorenz

1.1. Abstract

The purpose of this chapter is to introduce the reader into the research subject of this thesis. We present a general overview of the topics under investigation and discuss the state in a study of semiconductor laser dynamics. We start with the background and the most important definitions accepted in the chaos theory and laser systems. Afterwards, we describe the main objectives and the motivation of this work. Then, we describe the thesis structure and give conclusions of this chapter.

1.2. Chaos and Laser

Chaotic essentially differs from noise. Since a chaotic system is described by deterministic equations, irregular oscillations in this system are called *deterministic chaos*. Instead, random oscillations in a noisy system are referred to as *stochastic processes*. Chaos in lasers is a deterministic process described by nonlinear differential equations.

In 1963 Lorenz [1] numerically investigated the behavior of convective fluids in the atmospheric flow model and found that a nonlinear system described by three variables can exhibit chaotic dynamics. Despite a chaotic motion in deterministic systems has been discovered in the beginning of the early 1900s by a prominent French mathematician Henri Poincaré [2]. He was the first scientist who found the "sensitivity to initial condition." The Lorenz's founding had a revolutionary impact to further development of the *chaos theory* and its application to many areas of science. In his book, H. Poincaré wrote, "it may happen that small differences in the initial conditions produce very great ones in the final phenomena. A small error in the former will produce an enormous error in the latter. Prediction becomes impossible, and we have the fortuitous phenomenon." Modern research of chaos started from the study of irregular and complex dynamics of a nonlinear system developed by Lorenz. Chaos is not only a description of a different viewpoint of nonlinear phenomena but also itself a new area of science. The system evolves in a deterministic way and its current state depends on its previous state in a rigidly deterministic way, although the systems' output shows irregular variations. This is in contrast to a random system where the present observation has no causal connection to the previous one. In spite of the deterministic models, we cannot foresee the future of the output, since chaos is very sensitive to the initial conditions, as Poincaré pointed out, and each system behaves completely different from each other even if the difference of the initial state is very small.

Chaos is always associated with *nonlinearity*. Nonlinearity in a system simply means that the flow (derivative) of the system variables depends nonlinearly on the variables. Nonlinear property in a system does not always guarantee the occurrence of chaos, but some form of nonlinearity is required for chaotic dynamics. Chaos has been observed in various fields of engineering, physics, chemistry, biology, and even in economics. Though the fields are different, some of the chaotic systems can be characterized by similar differential equations. Since they show similar chaotic dynamics, the same mathematical tools can be applied to the analysis of their chaotic dynamics.

Chaos has been also found in optics. Many optical materials and devices exhibit a nonlinear response to the electro-magnetic field and, therefore, they are candidates for chaotic

systems. One such device is a laser. Since lasers are nonlinear systems and are typically characterized by three variables: field, polarization, and population inversion, they naturally demonstrate chaotic oscillations. Indeed, in the mid 70's Haken [3] proved the similarity of laser equations to the Lorenz model and demonstrated chaotic dynamics in their output powers. He considered a ring laser model with two-level atoms in the laser medium. Although his model does not always describe real lasers, the approximation is reasonable for most lasers. Thereafter, the laser rate equations of three variables are known as the Lorenz-Haken model [4]. However, not all lasers exhibit a chaotic behavior, but those of them, which have bad cavity conditions. In the meantime, chaos was theoretically demonstrated in a ring laser system [5]. Then, Weiss and Brocke [6] observed Lorenz-Haken chaos in infrared NH_3 lasers. Contrary to the Haken's prediction, ordinary lasers are stable systems and only optically-pumped infrared lasers showed a chaotic behavior. Later, Arecchi et al. [7] investigated a laser system from the viewpoint of the characteristic relaxation times of the three variables and categorized lasers into three classes. According to their classifications, one or two of the relaxation times are in general very fast compared with the other time scales, and most lasers are described by the rate equations with one or two variables. Therefore, they are stable systems, and they are classified into classes A and B. Only, class C lasers are described by rate equations with three variables and they can exhibit chaotic dynamics. Nevertheless, class A and B lasers can also show chaotic dynamics when additional degrees of freedom are introduced. In particular, class B lasers are characterized by the rate equations for field and population inversion, and they are easily destabilized by an additional degree of freedom induced by an external perturbation. For example, solid state lasers, fiber lasers, and CO_2 lasers belonging to class B lasers, display irregular oscillations when external or feedback light is injected into the laser or modulation is applied to a laser parameter. Semiconductor lasers, which also belong to class B lasers, are very sensitive to self-induced optical and opto-electronic feedback, optical injection from other lasers, and pump current modulation.

1.3. Historical overview of chaos research in semiconductor lasers

Semiconductor lasers described by the optical field and the carrier density (equivalently to the population inversion) equations, can be easily destabilized by the introduction of an additional degree of freedom in the forms of optical feedback, external optical injection, or modulation of laser parameters. Feedback induced instabilities and chaos in semiconductor extensively have been the subject of an intensive study since the early 80's, [8]. In a semiconductor laser, the light reflected back to the laser from an external reflector considerably affects the laser oscillation; varieties of dynamical regimes have been observed.

One of the main differences between semiconductor and other lasers is the low reflectivity of the internal mirrors of the semiconductor laser cavity, which typically ranges from 10 to 30% of the intra-cavity intensity in edge-emitting semiconductor lasers. This makes the feedback effects significant in semiconductor lasers. Another difference is a large absolute value of the linewidth enhancement factor α of the laser media; depending on the laser materials $\alpha = 2 \sim 7$ was reported, while α is almost zero in other types of lasers. Moreover, the coupling between the phase and the carrier density also influences on the laser dynamics. These factors lead to a very rich dynamics, quite different from any other lasers. At weak and moderate external optical feedback reflectivity, the laser output exhibits different dynamical regimes, such as stable emission, periodic and quasi-periodic oscillations, and chaos when a control parameter is varied. These regimes are useful for some practical applications of semiconductor lasers, such as optical data storage and optical communication. The extensive review on the semiconductor lasers with optical feedback can be found in the literature [9-12].

Optical injection adds an additional degree of freedom to semiconductor lasers that can induce chaotic oscillations in the laser output. It was numerically predicted [13,14] and experimentally demonstrated [15,16] that an optically injected semiconductor laser follows a period-doubling route to chaos. An additional degree of freedom can be also induced by pump current modulation [17], that controls the output power and, at the same time, the laser frequency.

Semiconductor lasers are rather unstable compared with other lasers, and their stabilization has been an important issue from the beginning of their discovery. An external perturbation can either stabilized or destabilized a semiconductor laser. Stabilization of semiconductor lasers is very important with regard to their applications. For example, frequency stabilization, linewidth narrowing, power stabilization, polarization fixing, and beam shaping are very important in optical communications, optical data storage systems, and optical measurements. In particular, ultra-stable semiconductor lasers are expected in broadband optical communications, high-precision optical measurements, and standard light sources.

In the following section, we will describe the main objectives of this thesis.

1.4. Objectives

The aim of this thesis is to investigate and analyze the dynamics that the optical injection induced in semiconductor lasers when they are coupled in different configurations. The work was initially motivated by the willing to know the role of different parameters that we can control in our configurations of some semiconductor lasers coupled, one of them is the coupling strength, and other is the bias current. Also, we want to analyze what type of synchronization properties has this two coupled systems. We study two different schemes: the first one is an experimental analysis of two mutually-coupled semiconductor lasers and the second one is an analytical study of three unidirectionally-coupled semiconductor lasers arranged in a ring using Lang-Kobayashi model.

The advantages of each configuration are described outline next:

The objective for the first configuration is experimentally study the intensity dynamics and the optical spectra of two mutually delay-coupled semiconductor lasers respect to the two relevant parameters of the coupled system, namely the bias currents and the coupling strength of the lasers. Moreover, the objective of the second configuration is to study a ring

of three unidirectionally-coupled semiconductor lasers with respect to the coupling strength and see what route to chaos will exhibit in the semiconductor lasers and what synchronization is presented in this configuration with this parameter of control.

This work is devoted to the investigation of the instabilities due to these two configurations between two and three semiconductor lasers coupled. The reasons for the convenience of such a study are multiple. First, for the configuration of two mutually coupled semiconductor lasers under the nonlinear dynamic vision, this scheme serves as an excellent tested model for some processes that we saw in Nature, i.e., the mutual interaction of two oscillators. It is worth to note that the reciprocal or bidirectional action between two systems should not be considered just as a double unidirectional problem. The intuition gained in studies of unidirectional schemes can easily fail when applied to a bidirectional configuration. In a mutually coupled situation, for instance, the time of the signal needs to come from one system to propagate up to the other might become a critical parameter. This is the case for semiconductor lasers. Due to the huge speed of the light, two SLs a few centimeters apart involve interaction delay times of the same order than the time scale of the SL dynamics, typically in the subnanosecond range. The fact that these two time scales are comparable makes the interaction delay time an extremely important consideration in the qualitative and quantitative behavior of the system. Second, from the application's point of view the study of the instabilities arising from the coupling of several SLs can produce some practical benefits. The coherent summation of the oscillations of the electric fields of many semiconductor lasers has been used for years as a simple way to obtain high-intensity laser beams, while locking is a key phenomenon in synchronization that is of interest in applications such as frequency stabilization and wavelength tunability. Optical bistability is another feature present in the mutually coupled scheme of two SLs and its use is of central importance for all-optical information processing techniques. Finally, a better understanding of chaotic synchronization in bidirectionally-coupled arrays of SLs can lead to new ideas and improvements in applying optical chaos for encryption purposes.

With this analysis we found that for two mutually coupled SLs, the semiconductor lasers show a regime of bistability (coexistence of LFF and CW) when we increase the coupling strength and the bias current is close to the current of threshold. We also observe significant modifications in the laser emission characterized via optical spectra, laser intensity dynamics, and cross-correlation when we change the bias current and the coupling strength of the lasers. Finally, we analyze the behavior of the lasers when we increase the number of lasers in a chain, where we found different scenarios of synchronization between pairs of lasers and the route to chaos that this lasers exhibit as a function of coupling strength.

Now, we are going to describe the next chapters that proceed in this thesis as follows:

1.5. Organization

This thesis consists of five chapters that can be read sequentially or independently. The flexibility in the writing of this work allows readers interested in specific information can go directly to Chapter of interest, without having read the previous chapters.

In Chapter 1, we describe the art of chaos research, with special emphasis in semiconductor lasers. With this, we establish an overview of chaos in laser systems. We also show the reasons why we want to analyze the injection optics in different configurations of semiconductor lasers coupled. Then we define the general and specific objectives of this research. Allow us to establish objectives and constraints focus of our project. Finally, we make a brief summary of the structure and organization of the thesis to guide readers interested in specific parts of this work

In chapter 2, we provide a broad overview of the work that will be further developed in the following chapters of this thesis. In this chapter, we will mostly present a summary of the main element on which this work is based, the semiconductor laser rate equations. We describe its operations and the derivations of semiconductor lasers. In addition, we discussed various chaotic dynamics in semiconductor lasers induced by optical injection. Finally, we presented what synchronization means and different types of synchronization that we are going to use in the next chapters.

In chapter 3, we experimentally revisit the dynamical behavior of two very similar mutually delay-coupled SLs. By analyzing the intensity dynamics and the highly resolved optical and frequency (rf) spectra, we study in detail the transition from stable continuous-wave (CW) regime to LFF, bistability (coexistence of LFF and CW) and chaos [14,16] when increasing the coupling strength. Particular attention is given to the synchronization of mutually coupled SLs in the regimes of LFF and coherence collapse. We also show that not only the laser dynamics but also the synchronization properties strongly depend on the laser bias currents. Finally, we present some conclusions based on the results obtained.

In Chapter 4, we investigate the dynamics of a system consisting of three unidirectionally-coupled semiconductor lasers in a ring configuration using the Lang-Kobayashi model. We analyze what route to chaos will a ring SLs exhibit while the coupling strength is increasing? In addition, how will the semiconductor lasers be synchronized on this route? In addition, we analyzed the stability of the system using a fixed-point analysis. Finally, we present some conclusions based on the results obtained.

In chapter 5, we present the main contributions and general conclusions of this research project and outline future work.

In the final part of this thesis are the appendices, with additional information such as definitions, a list of the instruments used for the experiment and the references of our published articles.

1.6. Conclusions

We presented a theory of chaos research in laser physics, especially in semiconductor lasers because this topic has been developed and studied in this work. Chaotic dynamics play an important role in semiconductor lasers, even for their solitary oscillations, and control of the dynamics is currently an important issue for practical applications. Another significant advance has been made in the area of chaotic optical secure communications. Chaotic secure communications using existing public optical communications links have been tested, and successful results have been obtained. For this reason in this chapter, we provide

to the reader a broad overview of the chaos in semiconductor lasers. First, we started with an antecedents and explanation of chaos in laser systems. Afterwards, we defined the overall objective of this research and we need to reach specific objectives to accomplish this thesis. Finally, we described the structure of the thesis to present a general overview of the topics we will discuss. I believe this thesis will be of interest not only to researchers in the field of laser chaos, but also to those working in nonlinear science and technology.

1.7. References

1. E. N. Lorenz, "Deterministic nonperiodic flow," J. Atoms Sci. vol. 20 (1963), 130–148.
2. H. Poincaré, The foundation of science: science and method. Science Press, Lancaster, 1913.
3. H. Haken, "Analogy between higher instabilities in fluids and lasers." Phys. Lett. vol. 53A (1975), 77–78.
4. H. Haken, Light, vol 2. North-Holland, Amsterdam, 1985.
5. K. Ikeda, "Multiple-valued stationary state and its instability of the transmitted light by a ring cavity system," Opt. Comm. vol. 30 (1979), 257–261.
6. C. O. Weiss and J. Brock, "Evidence for Lorenz-type chaos in a laser," Phys. Rev. Lett., vol. 57 (1986), 2804–2806.
7. F. T. Arecchi, G. L. Lippi, G. P. Puccioni and J. R. Tredicce, "Deterministic chaos in laser with injected signal". Opt. Comm., vol. 51 (1984a), 308–314.
8. R. Lang and K. Kobayashi, "External optical feedback effects on semiconductor injection properties," IEEE J. Quantum. Electron., vol. 16 (1980), 347–355.
9. G. H. M. Van-Tartwijk and G. P. Agrawal, "Laser instabilities: a modern perspective," Prog. Quantum. Electron., vol. 22 (1998), 43–122.

10. J. Ohtsubo, “Feedback induced instability and chaos in semiconductor lasers and their applications,” Opt. Rev., vol. 6 (1999), 1–15.
11. K. Otsuka, Nonlinear dynamics in optical complex systems. KTK Scientific Publishers, Tokyo, 1999.
12. J. Ohtsubo, Chaotic dynamics in semiconductor lasers with optical feedback. E. Wolf progress in optics, vol. 44, Amsterdam, 2002a.
13. J. Sacher, D. Baums, P. Panknin, W. Elsaßer and E. O. Gobel, “Intensity instabilities of semiconductor lasers under current modulation, external light injection, and delayed feedback,” Phys. Rev. A, vol. 45 (1992), 1893–1905.
14. V. Annovazzi-Lodi, S. Donati and M. Manna, “Chaos and locking in a semiconductor laser due to external injection,” IEEE J. Quantum Electron., vol. 30 (1994), 1537–1541.
15. T. B. Simpson, J. M. Liu, A. Gavrielides, V. Kovanis and P. M. Alsing, “Period doubling route to chaos in a semiconductor laser subject to optical injection,” Appl. Phys. Lett., vol. 64 (1994) 3539–3541.
16. T. B. Simpson, J. M. Liu, A. Gavrielides, V. Kovanis and P. M. Alsing, “Period doubling cascades and chaos in a semiconductor laser with optical injection,” Phys. Rev. A, vol. 51 (1995a), 418–4185.

Chapter 2. Lasers theory

"I was exhilarated.... I thought, `Wow, the laser is working!' But to tell you the truth, I was a little numbed. ... I did not appreciate the gravity of what I had done."

Theodore H. Maiman

2.1. Abstract

In this chapter, we review laser theory especially semiconductor lasers and then we derive the rate equations, which are the starting point of the study of chaotic dynamics in semiconductor lasers. The semiconductor laser described here is a Fabry-Perot type with a mono-layer active region. The relaxation oscillation frequency, which is calculated from the rate equations, plays an important role in the dynamics of semiconductor lasers. Some other fundamental characteristics of semiconductor lasers are also discussed.

2.2. Theory of lasers

2.2.1. Basic laser characteristics

Lasers are devices that produce intense beams of light which are *monochromatic*, *coherent*, and *highly collimated*. The wavelength of laser light is extremely pure (monochromatic) when compared to other sources of light, and all of the photons that make up the laser beam have a fixed phase relationship (coherence) with respect to one another. Light from a laser typically has very low divergence. Because of these properties, lasers are used in a wide variety of applications in all walks of life.

The word *laser* is the acronym for (L)ight (A)mplification by (S)timulated (E)mission of (R)adiation. The principle of the laser operation relies on the basis of quantum-mechanical interaction of matter (electrons) and light (photons). Electrically charged particles like electrons can bear additional energy, and that energy can be transferred by absorbing or emitting photons. In the process of absorption an electron in a state with energy E_1 absorbs a photon and goes into a state with energy E_2. The energy difference between the initial and the final state of the electron is equal to the photon energy hν, where h is the Planck's constant and ν the frequency of the photon.

$$E_2 - E_1 = \Delta E = h\nu. \tag{2.1}$$

2.2.1.1 The Bohr atom

In 1915, Neils Bohr proposed a model of the atom that explained a wide variety of phenomena that were puzzling scientists in the late 19th century. This simple model became the basis for the field of quantum mechanics and was very useful for demonstrating laser principles. In Bohr's model, shown in figure 2.1, electrons orbit the nucleus of an atom. Unlike earlier "planetary" models, the Bohr atom has a limited number of fixed orbits that are available to the electrons. Under the right circumstances an electron can go from its ground state (lowest-energy orbit) to a higher (excited) state, or it can decay from a higher state to a lower state, but it cannot remain between these states. The allowed energy states are called "quantum states" and are referred to by the principal "quantum numbers" 1, 2, 3, etc. The quantum states are represented by an energy-level diagram.

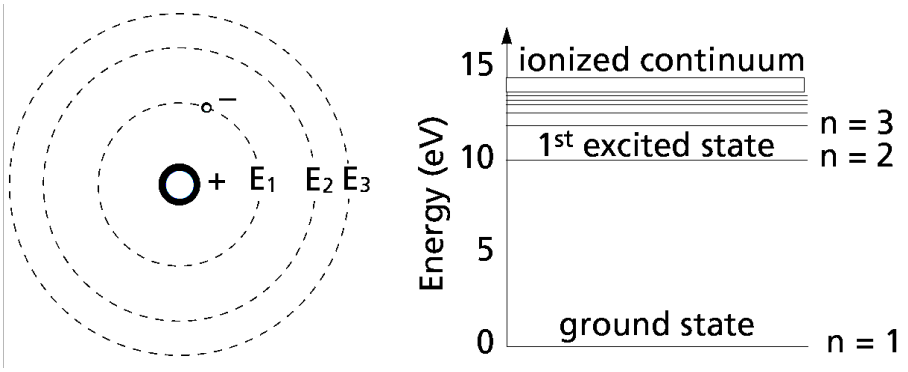

Figure 2.1 The Bohr atom and a simple energy-level diagram

2.2.1.2 Spontaneous and stimulated emission

In the process of stimulated emission an incident photon stimulates an electron (which must not be in its ground state) to emit a second photon. The emitted photon is an exact copy of the incident photon, they have the same frequency (and therefore the same energy), they are in phase, they have the same polarization, and they propagate in the same direction. This is opposed to spontaneous emission where a photon is emitted spontaneously, only driven by the tendency of the electron to go to a lower energy state. Absorption, spontaneous emission, and stimulated emission are illustrated in figure 2.2

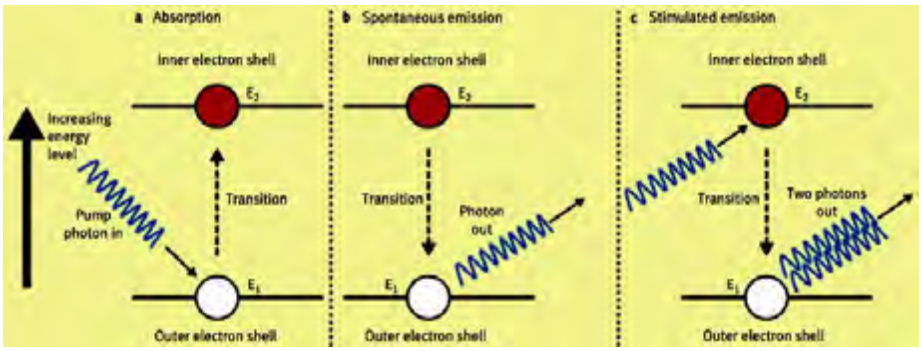

Figure 2.2 Spontaneous and stimulated emission

In this thesis, these individual processes are important in the sense that they will contribute to changes of the number of photons within the laser. The concept of stimulated emission as the reverse process of absorption was already postulated by Einstein in 1917 [1]. However, the technical realization of the laser was only achieved several decades. In 1960, Maiman reported to stimulate optical radiation in ruby in 1960 [2]. Of course, many other researchers had been working on amplification of light; a historical account of the invention of the laser can be found in textbooks such as Hecht in 1992 [3]. In order to amplify light by stimulated emission it is essential to have more electrons with higher energy than with low energy. This condition is called population inversion. To explain this concept we now consider the group of atoms shown in figure 2.3. All begin in exactly the same excited state, and most are effected within the stimulation range of a passing photon. The incoming (stimulating) photon interacts with the first atom, causing stimulated emission of a coherent photon; these two photons then interact with the next two atoms in line, and the result is

four coherent photons, on down the line. At the end of the process, we will have eleven coherent photons, all with identical phases and all traveling in the same direction. In other words, the initial photon has been "amplified" by a factor of eleven. Note that the energy to put these atoms in excited states is provided externally by some energy source which is usually referred to as the "pump" source.

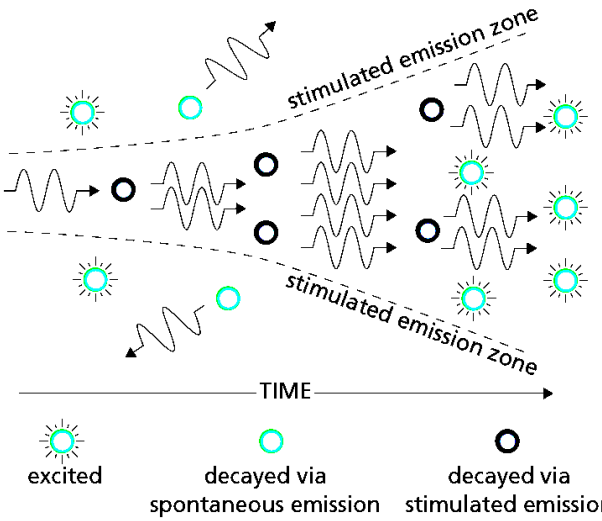

Figure 2.3 Amplification by stimulated emission

Of course, in any real population of atoms, the probability of stimulated emission is quite small. Furthermore, not all of the atoms are usually in an excited state; in fact, the opposite is true. Boltzmann's principle, a fundamental law of thermodynamics, states that, when a collection of atoms is at thermal equilibrium, the relative population of any two energy levels is given by

$$\frac{N_2}{N_1} = \exp\left[-\frac{E_2 - E_1}{kT}\right] \tag{2.2}$$

Where N_2 and N_1 are the populations of the upper and lower energy states, respectively, T is the equilibrium temperature, and k is Boltzmann's constant. The energy difference between the initial and the final state of the electron is equal to the photon energy hν, equation (2.1).

Substituting equation 2.1, we have

$$\Delta N \equiv N_1 - N_2 = \left(1 - e^{-h\upsilon/kT}\right)N_1 \tag{2.3}$$

2.2.1.3 The resonator

There are many types of lasers today; all have certain elements in common which are needed to achieve laser emission: a gain medium, a resonant cavity and a pumping system. These three elements are represented in Figure 2.4 and are called the resonator.

The optical resonant cavity is an arrangement of mirrors that forms a standing wave cavity resonator for light waves. Optical cavities are a major component of lasers, surrounding the gain medium and providing feedback of the laser light. The most common types of optical resonant cavities consist of two facing planes (flat) mirrors. The simplest of these is the Fabry–Perot cavity, consisting of two opposing flat mirrors. This arrangement is commonly used in microchip and microcavity lasers and semiconductor lasers due to they need a short cavity with a small mirror separation distance (L < 1 cm). The light confined in the cavity reflects multiple times producing standing waves for certain resonance frequencies. The standing wave patterns produced are called modes.

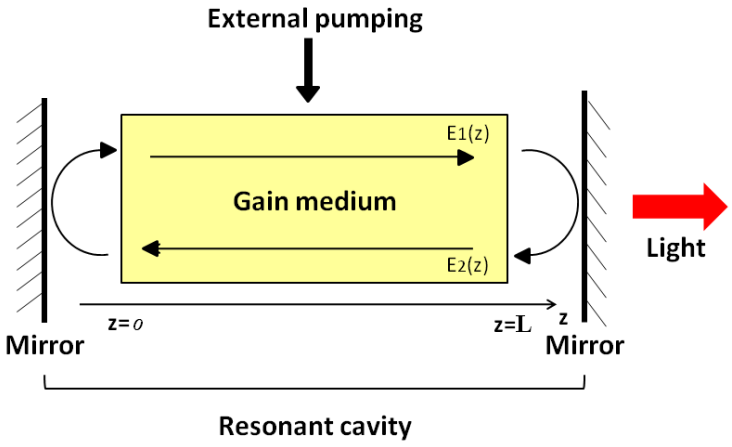

Figure 2.4 Sketch of a solitary laser. Fabry-Perot laser cavity with its main elements

The gain medium that features population inversion is called active medium. In an active material an incident photon, for example of a spontaneous emission process, can trigger a cascade of stimulated emissions of photons which are all in-phase.

2.2.1.4 Types of lasers

Since the discovery of the laser, literally thousands of types of lasers have been discovered. As Arthur Shaw low is purported to have said, “Hit it hard enough and anything will lase.” However, only a relative few of these lasers have found broadly based, practical applications. Lasers can be broadly classified into four categories: gas discharge lasers, semiconductor diode lasers, optically pumped lasers, and “other,” a category which includes chemical lasers, gas dynamic lasers, x-ray lasers, combustion lasers, and others developed primarily for military applications.

2.2.1.5 Semiconductor lasers

In a semiconductor laser the active medium is a semiconductor material. This active media is made by the union of n-type with p-type material. Atoms that belong to group VI of the periodic table, such as silicon and germanium, are used to form the main crystalline structure. In semiconductor lasers, the population inversion is achieved by injecting electrons into the conduction band. The union of n-type with p-type material is known as a diode.

2.2.1.6 Semiconductor media

Let us have a look at the distribution of charge carriers (electrons) between the conduction and the valence band in semiconductor materials [See Fig. 2.5]. The energy difference between both bands is called the band gap. Stimulated emission can occur when the energy of the incoming light exceeds the energy band gap of the semiconductor material.

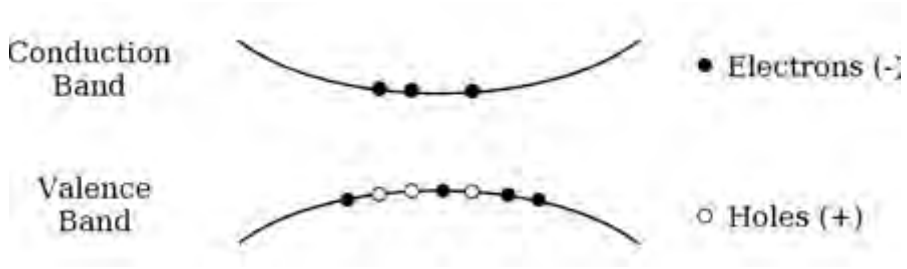

Figure 2.5 Electrons and holes in an arbitrary distribution between bands.

When an electron jumps from the valence band to the conduction band (see figure 2.5), it leaves behind what is called a "hole" (the absence of a charge carrier) in the valence band. The annihilation of an electron and a hole leads to spontaneous emission or stimulated emission when an extra photon is involved. By doping a semiconductor material one can alter the natural distribution of electrons and holes. A p-doped semiconductor has an excess of holes and a n-doped semiconductor an excess of electrons, originating from acceptors and donors respectively. At the junction of a p-doped and a n-doped doped semiconductor, stimulated emission dominates over absorption if there is population inversion. The semiconductor medium is transparent when the rates of stimulated emission and absorption are equal.

An incoming beam of photons experiences a gain in a p-n junction with population inversion, meaning that the number of outgoing photons is larger than the number of incoming photons. For this reason, this region is called the active layer of the laser.

A wide range of III-V material systems is used for the production of semiconductor lasers.

2.2.2 Semiconductor laser rate equations

Most lasers are typically described through three macroscopic variables consisting of the electric field, population inversion, and material polarization. Depending on the time scales in which the three variables decay, none of them, one, or even two of these variables may be adiabatically eliminated. A classification of lasers is made according to the number of

variables eliminated. Hence, Class C lasers are those in which the three decay variables are of the same order of magnitude and no adiabatic elimination of any of the variables proceeds. In this case, the three variables are needed to accurately describe the main physical processes in the laser. In Class B lasers, only one of the variables is eliminated and two of them are still required to capture the dynamics of the laser. Finally, in Class A lasers, only one variable governs the evolution of the system. Since in a semiconductor the relaxation time for the polarization is much shorter than for the rest of the variables, it can be adiabatically eliminated and the semiconductor laser falls into the Class B group.

The light-matter interactions occurring in a semiconductor laser can be modeled in a simple way using the well-known rate equations (RE) approach [4-7]. These equations describe the temporal evolution of the electric field and carrier density inside the laser cavity, and they predict many aspects of semiconductor laser behavior, including the output dynamics, frequency profile, and intensity versus current characteristics [8]. These equations are based on a travelling wave description of the electromagnetic fields inside the laser cavity.

The RE model consists of the charge and the optical field conservation equations. The optical field conservation equation can be represented by complex numbers, expressing the real and imaginary parts of the field ($E = E_x + iE_y$), or via its intensity (the number of photons per unit volume in the optical cavity) and the carrier density N (the number of charge carriers per unit volume in the active region).

The RE system is presented for a single mode laser and the analysis can be extended to multi-mode lasers, considering an equivalent set of equations for each optical mode. The physics of (bulk gain medium) Fabry-Perot semiconductor lasers can be modeled following a straightforward semiclassical approach.

The electric field vector, E, within the laser cavity is written

$$E = E_0 \exp\left[i(\omega t - kz)\right] + E_0^* \exp\left[-i(\omega t - kz)\right] \tag{2.4}$$

where ω is the angular frequency, and the complex propagation constant k is given by

$$k = n\frac{\omega}{c} - \frac{i\alpha_s}{2} \tag{2.5}$$

with n the real part of the refractive index, c the speed of light, and α_s is the absorption coefficient of the medium (which modifies the refractive index through the pumping mechanism). Using the travelling wave amplifier model, the resonator is considered as a Fabry-Perot cavity consisting of a dielectric medium of length L confined between two mirrors of reflectivity R_1 and R_2. The forward travelling and backward travelling complex electric fields then yield the condition for stationary laser oscillation

$$\sqrt{R_1 R_2}\,\exp\left[-2i\frac{n\omega}{c}L - \alpha_{abs}L\right] = 1 = G \tag{2.6}$$

For mirrors of reflectance $R_1 = r_1^2$ and $R_2 = r_2^2$, the wave intensity decreases by the factor R_1R_2 in the course of the two reflections associated with a single round trip. The overall intensity attenuation factor is therefore

$$r^2 = R_1 R_2 \exp(-2\alpha_s L) \tag{2.7}$$

This is usually written in the form

$$r^2 = \exp(-2\alpha_r L) \tag{2.8}$$

Where $\exp(-2\alpha_s L)$ is the round-trip power attenuation factor and α_r is an effective overall distributed-loss coefficient. Equations (2.7) and (2.8) provide [8]:

$$\alpha_r = \alpha_s + \frac{1}{2L}\ln\left[\frac{1}{R_1 R_2}\right] \tag{2.9}$$

This can also be written as

$$\alpha_r = \alpha_s + \alpha_{m1} + \alpha_{m2} \tag{2.10}$$

Represent the loss coefficient attributed to mirror 1and 2, respectively.

The loss coefficient can be cast in a simpler form for mirrors of high reflectance. If R_1=1, then $\ln(1/R_1) = -\ln(R_1) = -\ln[1-(1-R_1)] \approx 1-R_1$ where we have used the approximation $\ln(1-\Delta) \approx -\Delta$, which is valid for $|\Delta| << 1$. This allows us to write

$$\alpha_{m1} \approx \frac{1-R_1}{2L} \tag{2.11}$$

Similarly, if $R_2 \approx 1$, we have $\alpha_{m2} \approx 1 - R_1/2L$. If, furthermore, $R_1 = R_2 = R \approx 1$. Then

$$\alpha_{m1} \approx \alpha_s + \frac{1-R}{2L} \tag{2.12}$$

The cavity loss is described by the inverse photon lifetime

$$\tau_p = \frac{1}{c\alpha_r} \tag{2.13}$$

Finally, substituting (2.9) into (2.13), we obtain [8]

$$\tau_p = \frac{1}{c}\left[\alpha_s + \frac{1}{2L}\ln\left(\frac{1}{R_1 R_2}\right)\right]^{-1} \tag{2.14}$$

The Q factor of an optical resonator is related with the loss coefficient and can be determined by observing that stored energy is lost at the rate $c\alpha_r$. When the Q factor is large this means that the resonator has low losses and the mirrors have high reflectance. $R_1 = R_2 = R \approx 1$.

The lasing frequency of the m_{th} longitudinal mode of the lasing cavity is

$$\omega_{th,m} = m\frac{\pi c}{nL} \tag{2.15}$$

The dynamic analysis of semiconductor laser oscillations is modeled by a set of rate equations. These can derive from the travelling wave amplifier model, which considers the electric field with respect to time and the electromagnetic wave equation, which describes the propagation of optical fields inside the semiconductor medium [8-10]:

$$\nabla^2 E - \frac{\sigma}{\varepsilon_0 c}\frac{\partial}{\partial t}E - \frac{1}{c^2}\frac{\partial}{\partial t^2}E = \frac{1}{\varepsilon_0 c^2}\frac{\partial^2}{\partial t^2}P_{pol}\ , \tag{2.16}$$

where P_{pol} is the macroscopic polarization, ε_0 is the vacuum permittivity, and α is the surface charge. The travelling wave approach yields the same results as a more rigorous derivation starting from the complete semiconductor Bloch equations and Maxwell equations [11,12]. Substitution of the electric field equation 2.4 into equation 2.16, taking account of the dispersion induced change in the dielectric constant, ε, given by [8-10]

$$\varepsilon E = \left[\varepsilon(\omega)E_0 + i\frac{\partial \varepsilon}{\partial t}\right]\exp\left[i\left(\omega t - kz\right)\right] + \left[\varepsilon(\omega)E_0^* + i\frac{\partial \varepsilon}{\partial t}\right]\exp\left[-i\left(\omega t - kz\right)\right] \tag{2.17}$$

yields the following rate equations, which describe the temporal change in the electric field, E, and the carrier density, N, within the semiconductor active region

$$\frac{dE(t)}{dt} = \frac{1}{2}(1+i\alpha)\left[G_n\left(N(t)-N_0\right) - \frac{1}{\tau_p}\right]E(t) \tag{2.18}$$

$$\frac{dN(t)}{dt} = \frac{I}{e_c} - \frac{N(t)}{\tau_n} - G_n\left[N(t)-N_0\right]E\Big|^2 \tag{2.19}$$

$G_n(N(t)\text{-}N_0)$ is the carrier density dependent gain, τ_n is the carrier lifetime, α is the linewidth enhancement factor, I is the injection current density, and e is the electric charge.

The rate equations (2.18) and (2.19) have been derived following a number of simplifying assumptions. Firstly, the slowly varying envelope approximation is employed. This relies on the difference in time scales at which the electric field changes in time and space. In addition, it is considered that the electric field amplitude *E(t)* varies slowly compared to the optical carrier frequency ω. In the second order differential equation for the electric field, derived from the electromagnetic wave equation, the second derivatives can be discarded as they are very small compared with the first order terms

$$\frac{d^2}{dt^2} \langle\langle \ \omega \frac{d}{dt} \langle\langle \ \omega^2 \tag{2.20}$$

Many aspects of the static behavior of semiconductor lasers can be obtained from steady state solutions of the rate equations. These include the light current characteristics. The semiconductor laser threshold injection current I_{th}, is found from the carrier density rate equation,

$$I_{th} = eVR(n_{th}), \tag{2.21}$$

where V is the applied voltage and the recombination rate at threshold $R(n_{th})$ is determined from the gain at threshold carrier density.

The output optical frequency spectrum (longitudinal mode structure) of a semiconductor laser is determined by several factors. Due to the high gain available in semiconductor materials, semiconductor lasers can be made very small and their cavity lengths are typically 100 to 1000μm and this result in very large longitudinal mode spacing, typically 50-500 GHz. However, because the transitions are between atomic semiconductor bands as opposed to discrete atomic energy , the gain bandwidth is also very large (10-100 nm). Hence, there are a large number of possible lasing modes under the gain curve. For a purely homogenously broadened linear gain medium, only one of these modes can lase. Such a single-frequency output would be ideal for the majority of applications. However, most

early semiconductor lasers and devices of simple construction typically operate on many longitudinal modes simultaneously.

The parameter α in (2.18) is an important parameter in semiconductor lasers, known as a linewidth enhancement factor, and plays a crucial role for laser oscillations. This term arises because the real refractive index of the active laser medium (n) varies with changing carrier density. Spontaneous emission events induce an instantaneous phase change in the laser field. Accompanying this phase change there is an instantaneous change in the laser field intensity, which results in a delayed phase change. In order to restore the steady state field intensity, the laser undergoes relaxation oscillations, which cause a deviation of the imaginary part of the refractive index (n''), from its steady state value. This change is caused by a changing carrier density, which also modifies the real part of the refractive index. The ratio of these fluctuations gives the linewidth enhancement factor [12,14]

$$\alpha = \frac{\Delta n}{\Delta n''} \tag{2.22}$$

This strong coupling of the carrier density to the refractive index is a characteristic of semiconductor lasers, where α is typically 2-5 for semiconductor lasers [15] and zero for other laser types, such as gas lasers. It influences many characteristics of semiconductor laser behavior, such as dynamics, modulation, noise, and linewidth. The typical feature of semiconductor lasers is a broad linewidth of laser oscillations due to a non-zero α parameter. The relaxation oscillations manifest themselves on the optical frequency spectrum as a set of sidebands separated from the central lasing mode by the relaxation oscillation frequency [16]. This frequency scale as the square root of the output power; typical values near maximum output power are 2-10 GHz [17].

A solitary semiconductor laser cannot exhibit chaotic dynamics because at least three ordinary differential equations are required in order to observe that complex behavior, and only two equations are coupled in the system of Equations (2.18) and (2.19). However, the effect of external perturbations on the semiconductor laser introduces additional degrees of freedom able to excite very rich complex dynamical states as bistability, excitability, or chaos. Among the diversity of ways of perturbing a laser, we point out the injection of light

into the active region of the laser, the feedback of light from the same laser into its own active region, and the modulation of the current supply. Any of these modifications of the solitary laser setup is subject to a great deal of analysis by the researchers because of intrinsic and applications interests. In this work, we study another kind of perturbation that consists of the mutual coupling of two semiconductor lasers allowing us to study the phenomenon of synchronization, which is introduced in the next section.

2.2.3. Dynamics in semiconductor lasers with optical injection

Since the semiconductor laser has unique features of high gain, low facet reflectivity, and amplitude-phase coupling through the α parameter, it is also sensitive to optical injection from a different semiconductor laser. A semiconductor laser with optical injection is an excellent model for generating chaos in its output power and the system has proven to be very useful in practical applications; the general application of optical injection is to control the laser. The optical injection technique is originally developed for the stabilization of the injected slave semiconductor laser, so that, at first glance, it may be surprising that the laser is destabilized by the optical injection. However, optical injection to a laser is an introduction of one extra degree of freedom from a viewpoint of nonlinear dynamics and the perturbed laser is a candidate of a chaotic system. In this section, we focus on the dynamics of optical injection effects in semiconductor lasers.

The process of optical injection is illustrated in figure 2.6 a single-frequency signal from a master source is injected into the active region of the slave laser. The master laser is optically isolated from the slave laser typically by a polarization dependent optical isolator. Similar to optical feedback, such optical injection has a variety of effects on the operating characteristics of the slave laser. It can induce various dynamic instabilities and chaotic behavior, lock the two lasers together in phase and frequency (injection locking), or excite the relaxation oscillation frequency of the slave laser.

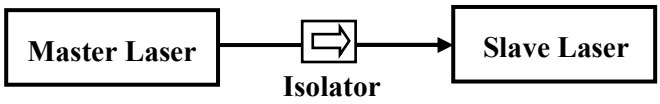

Figure 2.6 Optical injection systems in semiconductor lasers

A dynamic analysis of a semiconductor laser subject to optical injection and optical feedback is achieved via the semiconductor rate equations. The rate equations describe the semiconductor laser dynamics in continuous wave operation.

The Lang–Kobayashi paper has become synonymous with the theoretical model, and this model extends the equations 2.18 and 2.19. This model of Lang-Kobayashi attempts to describe the behavior of single-mode semiconductor lasers subject to external optical feedback (for a complete derivation of this model see [18]). This widespread application of the model is explained rather simply in terms of its remarkable ability to describe almost all salient experimental features of a semiconductor laser subject to optical feedback. In the case of optical injection, the Lang-Kobayashi equations are modified to account for the interaction of the slave laser electric field with the electric field of the master laser, within the slave laser active layer. Therefore, we insert the injection rate into the equation (2.18) and take into consideration the lag of the external cavity for the amplitude of the complex field. The equations read [19]:

$$\frac{dE_{master}(t)}{dt} = \frac{1}{2}(1+i\alpha)\left[G_n\left(N(t)-N_0\right)-\frac{1}{\tau_p}\right]E(t)+\underbrace{kE_{slave}(t-\tau)\exp(-i\omega_0\tau)}_{\text{Injection term}}, \qquad (2.23)$$

$$\frac{dN(t)}{dt} = \frac{I}{e_c}-\frac{N(t)}{\tau_n}-G_n\left[N(t)-N_0\right]\left|E\right|^2 \qquad (2.24)$$

Where τ is the round trip time of light in the external cavity as introduced before, k is the coupling strength, and ω_0 is the optical frequency. The injection term $E(t\text{-}\tau)exp(\text{-}i\omega_0\tau)$ takes the amount of injection and the phase after one external cavity round trip into account. Solution of the above rate equations yields the dynamic state of the slave laser depends on the injected signal power and detuning.

In the next section of this chapter, we are going to develop the concepts of synchronization, and the presentation of the different hallmarks and measurements of synchronization.

2.3. Synchronization

In 1665, the great Dutch scientist Christian Huygens first noticed the fundamentals of the synchronization phenomena, which will be studied in this section for interacting semiconductor lasers. While sick and staying in bed for a couple of days watching two clocks hanging on a common support, Huygens observed "a wonderful effect that nobody could have thought before."

> *... It is quite worth noting that when we suspended two clocks so constructed from two hooks embedded in the same wooden beam, the motions of each pendulum in opposite swings were so much in agreement that they never receded the least bit from each other and the sound of each was always heard simultaneously.*

This historical example of synchronization and many other phenomena can be understood within the unifying framework of the nonlinear sciences. We will start by defining what we mean synchronization in the language of the nonlinear dynamics.

2.3.1 Synchronization phenomenon

Synchronization is the dynamical process by which two or more oscillators adjust their rhythms due to a weak interaction [20]. Part of the universality of this phenomenon comes from the vast variety of systems able to experience this effect.

The synchronization depends on the strength of the interaction. The interaction or coupling between two oscillators can occur through rather complex mechanisms. Where, a small set of parameters that control the intensity of the interaction, namely the coupling strength. Thus, the coupling rate regulates how strong an oscillator affects the motion of another. Of course, the mutual interaction needs not to be symmetric. The extreme case of asymmetric coupling corresponds to a unidirectional influence of one oscillator to another.

2.3.2 Different kinds of synchronization

Several types of synchronization have been reported in the literature depending on the relationship that the signals $x_1(t)$, and $x_2(t)$ of two interacting systems may exhibit. Recently, the word synchronization has gained popularity in the nonlinear dynamics literature [21].

Below, the most important characteristics of the different kinds of synchronization are summarized.

In chaotic systems, one can distinguish the following types of synchronous motion:

• ***Identical or complete synchronization.***

The simplest case occurs when two coupled systems generate an identical output, $x_1(t) = x_2(t)$. Far from trivial, it was noticed that this phenomena could be observed even in chaotic systems. In general, this exact solution only exists for identical chaotic oscillators [22-24].

Curiously, not always, a stronger interaction between the subsystems leads to a more stable synchronization manifold, but synchronization is only stable in a given range of coupling strengths. Regarding this issue, Pecora and Carroll, in Refs. [25,26], devised a master stability function that is capable of predicting the desynchronization thresholds and size limits for an identical synchronization of an array of linearly coupled systems.

• ***Generalized synchronization.***

This type of synchronization attempts to capture a more general relation between two coupled systems. Generalized synchronization is usually defined as the existence of a smooth and invertible mapping $F : x_2(t) = F [x_1(t)]$ between the trajectories of two coupled chaotic dynamical systems [27]. Some authors distinguish between strong and weak synchronization depending on this mapping F being smooth or not [28]. More recently, the definition of generalized synchronization has been extended to a general functional relation $F(x_1, x_2) = 0$ between the states of two coupled oscillators [29]. In unidirectional coupled

systems this type of synchronized solution has a clear interpretation; it means that the state of the slave system can be completely determined or predicted by observing the master. Commonly, the task of proving the existence of generalized synchronization in a system is much easier than finding the actual function that relates both outputs. In particular, the auxiliary approach suggested by Abarbanel et al. [30,31] provides a simple test to check the existence of generalized synchronization.

• ***Phase synchronization.*** Since the phase of an oscillator is much more sensitive to perturbations than its amplitude, for low coupling strength two interacting oscillators can achieve an entrainment of their phases with the interaction hardly affecting their amplitudes. Phase synchronization expresses the regime where the phase difference between two irregular oscillators is bounded but their amplitudes remain uncorrelated [32]. The term *phase synchronization* is usually referred to the case in which the phase difference between the two outputs is bounded but their amplitudes stay uncorrelated

• ***Lag synchronization***. This type of synchronization takes into account relations between two systems when compared at different times [21]. The manifestation of relations such as $x_1(t) = x_2(t - \tau)$ due to a coupling between the two systems is claimed as a lag synchronization. For positive (negative) τ the system 1 is said to lag (advance) the dynamics of system 2. This type of synchronization may appear in instantaneously coupled systems [33] but is prominent in cases where the interaction time between subsystems needs to be taken into account [34]. Anticipated synchronization is a special type of lag synchronization. When system 1 affects unidirectionally to system 2, and still the latter is able to advance the dynamics of the first one [34], we call this counterintuitive process anticipated synchronization. The most common scheme to observe anticipatory synchronization is when the transmitter is affected by a feedback long loop [35]. In this way, it is possible for the receiver to be influenced by the transmitter sooner than the transmitter is affected by its own feedback, and thus the receiver can advance the dynamics of the transmitter without violating causality [36, 37].

2.3.3 Cross-correlation function

The degree of quality of most types of synchronizations (identical, localized, and lag) is usually measured by computing indicators such as the cross-correlation function [38]

$$C(\Delta t) = \frac{\left\langle \left[I_1(t) - \langle I_1 \rangle \right] \left[I_2(t + \Delta t) - \langle I_2 \rangle \right] \right\rangle}{\left\{ \left\langle \left[I_1(t) - \langle I_1 \rangle \right]^2 \right\rangle \left\langle \left[I_2(t) - \langle I_2 \rangle \right]^2 \right\rangle \right\}^{1/2}} \tag{2.18}$$

where I_1 and I_2 are the output intensity of laser 1 and laser 2, respectively. Angle brackets < > denote time average, and Δt is the time shift. This indicator is used in our study to characterize the synchronization between two semiconductor laser outputs.

2.4. Conclusions

The laser as a directed, high brightness, coherent source of light was a dream come true at its demonstration in 1960. A jump of several orders of magnitude improvement towards the ideal of a single frequency, 'zero' linewidth, spatially coherent, plane wave source of light had been made. A major new research field in physics and engineering was the development of different types of lasers, aiming to cover that part of the electromagnetic radiation spectrum that can be called 'light', grew rapidly. Almost any laser can be made to generate an output that is unstable in time by optical injection or optical feedback. Semiconductor lasers are susceptible to instabilities induced by optical injection and these can also be used to improve many of the operating characteristics. These instabilities make the output of semiconductor lasers more appropriate for many applications.

The nonlinear characteristics of the semiconductor laser systems are of interest both in their own right and in contrast to other biological, mechanical, hydro dynamical and electronic nonlinear systems. They also contrast with the nonlinear dynamics of other laser systems because of the high frequencies and small time scales (picoseconds) involved. The potential applicability of chaotic semiconductor lasers, when synchronized in pairs or arrays in optical communications has given a strong application based motivation for fully exploring

the nature of chaotic outputs from semiconductor lasers with optical injection. We can find semiconductor laser in many applications which include, apart from telecommunications, holography, printing, welding, reading and recording discs, optical pumping of other lasers, material processing, etc.

In this chapter, we presented a brief summary of the main element on which this work is based, the semiconductor laser. We described its operation and the derivation of semiconductor laser rate equations. This chapter discussed various chaotic dynamics in semiconductor lasers induced by optical injection. Finally, we presented what synchronization means and different types of synchronization that we are going to use in the next chapters.

2.5 References

1. A. Einstein, "Zur quantentheorie der strahlung," Phys. Z., vol. 18 (1917), 121–128.
2. T. H. Maiman. "Stimulated optical radiation in ruby," Nature, vol. 187 (1960), 493–494.
3. J. Hecht. Laser pioneers. Academic press inc., San Diego, 1992.
4. H. Haken, Light, vol. 2, North-holland, Amsterdam, 1985.
5. G. P. Agrawal and J. T. Klaus, "Effect of phase-conjugate feedback on semiconductor laser dynamics," Opt. Lett., vol. 17 (1991), 1325-1327.
6. G. P. Agrawal. Fiber-Optic Communication Systems. John Wiley & Sons, Inc., 2002.
7. L. A. Coldren and S. W. Corzine. Diode Lasers and photonic integrated circuits. John Wiley & Sons, Inc., 1995.
8. E. A. Saleh Bahaa, M. C. Teich. Fundamentals of photonics, John Wiley & Sons, Inc., chap. 9, 1991.

9. K. Petermann, Laser diode modulation and noise, Kluwer academic publishers, Dordrecht, 1988.
10. G. H. M. Van-Tartwijk and G. P. Agrawal, “Laser instabilities: a modern perspective,” Prog. Quantum Electron., vol. 22 (1998), 43-122.
11. G. H. M. Van-Tartwijk and D. Lenstra, “Semiconductor lasers with optical injection and feedback,” Quantum Semiclass. Opt., vol. 7 (1995), 87-143.
12. H. Henry, “Theory of the linewidth of semiconductor lasers,” IEEE J. Quantum Electron., vol. QE-18 (1982), 259-264.
13. S. Saito, O. Nilsson, and Y. Yamamoto, “Oscillation center frequency tuning, quantum FM noise, and direct frequency modulation characteristics in external grating loaded semiconductor lasers,” IEEE J. Quantum Electron., vol. QE-18 (1982), 961-970.
14. M. Osinski and J. Buus, “Linewidth broadening factor in semiconductor lasers an overview,” IEEE J. Quantum Electron., vol. QE-23 (1987), 9-28.
15. F. Favre, D. Guen, and J. C. Simon, “Optical feedback effects upon laser diode oscillation field spectrum,” IEEE J. Quantum Electron., vol. QE-18 (1982), 1712-1717.
16. H. Henry, “Theory of the phase noise and power spectrum of a single mode injection laser,” IEEE J. Quantum Electron., vol. QE-19 (1983), 1391-1397.
17. K. Kikuchi and T. Okoshi, “Measurement of FM noise, AM noise, and field spectra of 1.3 μm InGaAsP DFB lasers and determination of the linewidth enhancement factor,” IEEE J. Quantum Electron., vol. QE-21 (1985), 1814-1818.
18. R. Lang and K. Kobayashi, “External optical feedback effects on semiconductor injection laser properties,” IEEE Journal of Quantum Electron., vol. QE-16 (1980), 347–355.

19. T. Heil, Ph.D. Thesis: Delay dynamics in semiconductor lasers. Feedback and coupling instabilities, stabilization, and synchronization, Shaker Verlag, Darmstadt, 2001.
20. A. Pikovsky, M. Rosenblum, and J. Kurths. Synchronization: A universal concept nonlinear science. Cambridge University Press, 2002.
21. S. Boccaletti, The synchronization dynamics of complex systems. Elsevier, New York University, 2008.
22. L. M. Pecora and T. L. Carroll, "Synchronization in chaotic systems," Phys. Rev. Lett., vol. 64 (1990), 821-823.
23. S. Boccaletti, L. M. Pecora, and A. Pelaez, "Unifying framework for synchronization of coupled dynamical systems," Phys. Rev. E, vol. 63 (2001), 0662191-4.
24. L. M. Pecora, T. L. Carroll, G. A. Johnson, D. J. Mar and J. F. Heagy, "Fundamentals of synchronization in chaotic systems, concepts and applications," Chaos, vol. 7 (1997), 520-524.
25. L. M. Pecora and T. L. Carroll. "Master stability functions for synchronized coupled systems," Phys. Rev. Lett., vol. 80 (1998), 2109-2111.
26. K. Fink, G. Johnson, T. Carrol, D. J. Mar, and L. Pecora. "Three coupled oscillators as a universal probe of synchronization stability in coupled oscillator arrays," Phys. Rev. E, vol. 61 (2000), 5080-5084.
27. N. Rulkov, M. Sushchik, L. S. Tsimring, and H. Abarbanel. "Generalized synchronization of chaos in directionally coupled chaotic systems," Phys. Rev. E, vol. 51 (1995), 980-984.
28. K. Pyragas. "Weak and strong synchronization of chaos," Phys. Rev. E, vol. 54 (1996), 4508-4511.

29. L. Kocarev and U. Parlitz. “Generalized synchronization, predictability, and equivalence of unidirectionally coupled dynamical systems,” Phys. Rev. Lett., vol. 76 (1996), 1816-1819.
30. H. D. I. Abarbanel, N. F. Rulkov, and M. M. Sushchik. “Generalized synchronization of chaos: The auxiliary system approach,” Phys. Rev. E, 53 (1996), 4528-4512.
31. Z. Zheng, X. Wang and M. C. Cross. “Transitions from partial to complete generalized synchronizations in bidirectionally coupled chaotic oscillators,” Phys. Rev. E, vol. 65 (2002), 056211-5.
32. M. Choi, K. V. Volodchenko, S. Rim, W. H. Kye, and C. M. Kim. “Transition from phase synchronization to complete synchronization in mutually coupled nonidentical nd:yag lasers,” Opt. Lett., vol. 28 (2003), 1013-5.
33. M. Zhang, G. M. Wei, and C. H. Lei. “Transition from intermittency to periodicity in lag synchronization in coupled rossler oscillators,” Phys. Rev. E, vol. 65 (2002), 036202-6.
34. H. U. Voss. “Anticipating chaotic synchronization,” Phys. Rev. E, vol. 61 (2000), 5115-9.
35. S. Tang and J. M. Liu. “Experimental verification of anticipated and retarded synchronization in chaotic semiconductor lasers,” Phys. Rev. Lett., vol. 90 (2003), 194101-3.
36. C. Masoller. “Anticipation in the synchronization of chaotic semiconductor lasers with optical feedback,” Phys. Rev. Lett., vol. 86 (2001), 2782-4.
37. M. Cisjak, O. Calvo, C. Masoller, C. R. Mirasso, and R. Toral. “Anticipating the response of excitable systems driven by random forcing,” Phys. Rev. Lett., vol. 90 (2003), 204102-4.

38. M. C. Soriano, F. Ruiz-Oliveras, P. Colet, and C. R. Mirasso, “Synchronization properties of coupled semiconductor lasers subject to filtered optical feedback,” Phys. Rev. E, vol. 78 (2008), 0462181-5.

Chapter 3. Spectral properties and synchronization scenarios of two mutually delay-coupled semiconductor lasers

---

"Science is built up of facts, as a house is built of stones; but an accumulation of facts is no more a science than a heap of stones is a house."

Henri Poincaré

3.1. Abstract

We experimentally study the intensity dynamics and the optical spectra of two similar mutually delay-coupled semiconductor lasers. While changing two relevant parameters of the coupled system, namely the bias currents and the coupling strength of the lasers, we observe significant modifications in the laser emission characterized via optical spectra, laser intensity dynamics, and cross-correlation functions. We find distinct synchronization scenarios for two bias currents: 1.02 and 1.25 times the threshold bias current of the solitary laser. Optical spectra in both cases strongly depend on the coupling strength between the

lasers. For the low bias current and strong coupling, the lasers exhibit dynamical bistability, i.e. the coexistence of low-frequency fluctuations and stable continuous-wave emission.

3.2. Introduction

Semiconductor lasers (SLs) subject to delayed feedback, as well as motifs of delay-coupled SLs have attracted much attention due to their potential applications in different areas, such as high-power emission by diode laser arrays [1], quantum noise reduction [2], chaotic communications [3,4], random number generation [5-7], and information processing [8] (for a review see [9]). In delay-coupled SLs, even short coupling delay times (1 ns or smaller) cannot be neglected due to the laser's fast characteristic time scales [10-12]. If the time taken by the light to travel from one laser to the other is of the same order of or larger than the relaxation oscillation period, a very rich dynamical behavior including fully developed chaos, low-frequency fluctuations (LFF), and coexistence of LFF and stable emission can be observed. This scenario is similar to that detected in a laser with delay optical feedback [13,14].

Although many researchers considered unidirectionally coupled semiconductor lasers [3,15,18], there is also a strong interest in studying mutually coupled SLs [10-12,19-24] where some unexpected dynamical behaviors were found [21,22]. One prominent aspect is the occurrence of a spontaneous symmetry breaking [10,11,19] that gives rise to stable *generalized achronal synchronization* in two mutually delay-coupled SLs [10,19,24]. This generalized achronal synchronization state is particularly interesting because it originates from the bidirectional coupling of perfectly symmetric systems. *Identical isochronal (zero-lag*) *synchronization* only occurs when self-feedback is added to each laser [25,26] or another laser or a semitransparent mirror is placed between the two SLs [27,28]. Although many studies addressed the dynamical and synchronization properties of mutually delay-coupled SLs, only few works included the study of their optical spectral properties [29,30]. Interestingly, it was found that their spectra present features similar to those of a solitary SL with optical feedback [31-35]; in particular, a significant line broadening is detected

when the lasers operate in a chaotic regime [33].

In this work, we experimentally revisit the dynamical behavior of two very similar mutually delay-coupled SLs. Our study is motivated by the recent availability of a new generation of instruments, such as high-resolution optical analyzers and high-speed real-time digital oscilloscopes that enable the characterization of the dynamical properties of delay-coupled SLs with unprecedented precision. By analyzing the intensity dynamics and the highly resolved optical and frequency (rf) spectra, we study in detail the transition from stable continuous-wave (CW) regime to LFF, bistability (coexistence of LFF and CW) and chaos [14,36] when increasing the coupling strength. Particular attention is given to the synchronization of mutually coupled SLs in the regimes of LFF and coherence collapse. We also show that not only the laser dynamics but also the synchronization properties strongly depend on the laser bias currents.

3.3. Experimental setup

The experimental arrangement is shown in Fig. 3.1. We used two fiber-pigtailed discrete-mode semiconductor lasers (Eblana Photonics), both with a 1542 nm nominal emission wavelength. The lasers were selected from the same wafer in order to achieve well-matched parameters, and butterfly mounted with Thorlabs mount LM14S2. Both the pump current and the laser temperature were controlled and stabilized by a Thorlabs PRO800 module ITC8022 with an accuracy of ±0.01°C and ±0.01 mA, respectively. The threshold current of the solitary laser 1 was I_{th1} = 11.28 mA at 19°C and that of laser 2 was I_{th2} = 11.85 mA at 20 °C. When the laser are coupled and the bias current is close to the lasing threshold, specifically, at I = 1.02 I_{th} their maximum value of power was $P_{1,2}$ = 21 μW and when the bias current is I = 1.25 I_{th} the maximum value of power of the lasers was $P_{1,2}$ = 69 μW; this values were taken from the remaining 10% output used for detection.

As shown schematically in Fig. 3.1, the lasers were connected via 90/10 optical couplers (OC_1 and OC_2). About 90% of the output radiation was used for the coupling through a polarization controller (PC) to ensure parallel polarization and the remaining 10% was used for detection by fast photodiodes (D) (Miteq 12.5-GHz bandwidth). The signals from the photodiodes were analyzed with a frequency spectrum analyzer (Anritsu MS2667C with a 9 kHz to 30 GHz frequency range) and a fast oscilloscope (LeCroy WaveMaster 8 16Zi with a sampling rate of 40 Gsamples/s and 16-GHz analog bandwidth). The optical spectra were measured with a high-resolution optical spectrum analyzer (BOSA with a 10MHz resolution). The round trip of the coupling time is $2\tau_c$ and the single coupling time was fixed to $\tau_c = nL/c = 63$ ns. Where $L_{\tau c} = 12.6$ m is the fiber length, c is the speed of light in vacuum, and n=1.5 the fiber refractive index. In order to protect the lasers from undesired feedback, optical isolator (ISO) were located in front of each photodiode. We use a single mode fiber (SMF28), and the fiber connectors were of APC type (connector with angle polished) and had a return loss of about 50 dB.

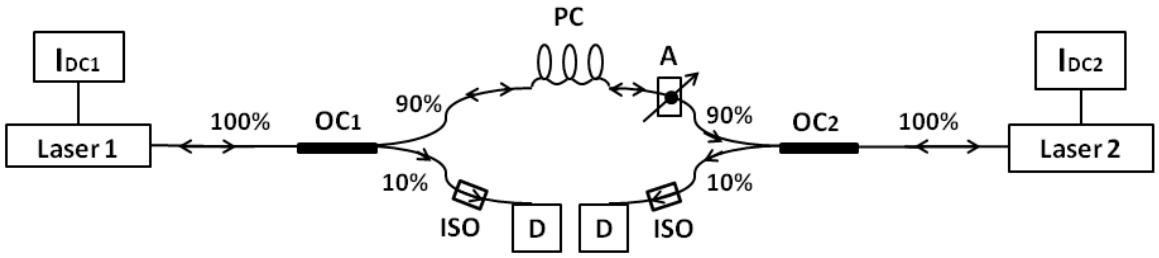

Figure 3.1. Experimental setup of two mutually coupled semiconductor lasers. I_{DC1} and I_{DC2} are laser current and temperature controllers, OC_1 and OC_2 are optical couplers, PC is a polarization controller, A is a variable attenuator, ISO are optical isolators, and D are photodetectors. All components are connected via optical fibers.

The dynamics and synchronization properties of delay-coupled SLs depend on several parameters, including injected powers and detuning of the laser wavelengths. In order to control the amount of light coupled to the lasers, we placed an attenuator (A) by which we varied the transmission losses between the lasers. In our experiments, the maximum

coupling was estimated by taking into account the coupling efficiency of the laser to the fiber that was approximately 75%, and to the optical couplers that was about 90% of transmission. Since we used two couplers and two fiber-pigtailed lasers, the whole coupling loss was about 45% (0.75×0.9×0.9×0.75). For the overall coupling strength, we had to add an extra 10% loss in the fiber connectors, and hence, the estimated maximum coupling was about 40% of the emitted light, which corresponds to approximately ~3 to 4 dB. The maximum coupling between the two mutually coupled semiconductor lasers corresponds approximately to ~30 to 35 dB, defined (1) by coupling losses between semiconductor lasers and the single mode fiber and (2) by the loss of splices and fiber optic multiplexers.

Before exploring the dynamics of the two mutually coupled SLs, we ensured that the lasers were as similar as possible and operated under the same conditions. Both the bias current and the temperature of each solitary laser were adjusted such that the uncoupled lasers had the same emission wavelengths and the same relaxation oscillation frequencies. The maximum and minimum coupling correspond to the loss of the attenuations of 0 dB and -34 dB of the laser emission, respectively. In the following sections, we study the laser dynamics for two different values of the bias currents: (i) when the laser is biased at $I = 1.02\ I_{th}$, and (ii) when the laser is biased at $I = 1.25\ I_{th}$, where I_{th} is the threshold current of the solitary lasers.

3.4. 3. Laser behavior for $I = 1.02\ I_{th}$

In this section we study the dynamics of the two mutually coupled SLs when the bias current is close to the lasing threshold, specifically, at $I = 1.02\ I_{th}$.

3.4.1. Intensity dynamics, optical and frequency (rf) spectra

Figure 3.2 shows optical spectra, intensity time series, and frequency (rf) spectra for different attenuation values (k). Similarly to a SL with optical feedback [31], four distinct

dynamical regimes are found depending on the coupling strength (or attenuation), that we describe as follows.

(i) The uncoupled and weakly coupled lasers operate in a noisy CW (stable steady state) regime characterized by a narrow spectral linewidth (k=-34 dB) [Fig. 3.2 (a)].

(ii) As the attenuation is decreased (k=-24 dB), the lasers start to oscillate in a chaotic manner; this process is accompanied by the linewidth broadening [Fig. 3.2 (b)]. Two dominant frequencies in the laser oscillations can be distinguished in the rf spectrum [right panel of Fig. 3.2 (b)]. The frequency corresponding to the interference between compound cavity modes is about $1/2\tau_c$ ~ 7.9 MHz [see spacing between frequency peaks at the inset figure in the right panel of Figure 3.2 (b)], while the relaxation oscillation frequency of the coupled lasers is about 3 GHz.

(iii) The linewidth further broadens when the injected power is increased, i.e., when the attenuation is decreased (k = -10 dB). The maxima in the optical and rf spectra shift towards smaller frequencies [Fig. 3.2 (c)]. This regime, known as coherence collapse, is characterized by a significant linewidth broadening by several orders of magnitude (to about 20 GHz) [33,36]. The laser oscillations again show two dominant frequencies.

(iv) At very strong coupling (k = -2 dB), bistability emerges [14,37]. The lasers operate either in the regime of LFFs [Fig. 3.2 (d)] or in a stable steady state of the compound cavity (CW regime) [Fig. 3.2 (e)]. These two stable states alternate in time due to the influence of spontaneous emission and carrier noise. In the steady state regime, the coherence of the lasers is regained, but the optical frequency is shifted towards smaller frequencies compared to the solitary lasers and the relaxation oscillations are strongly suppressed.

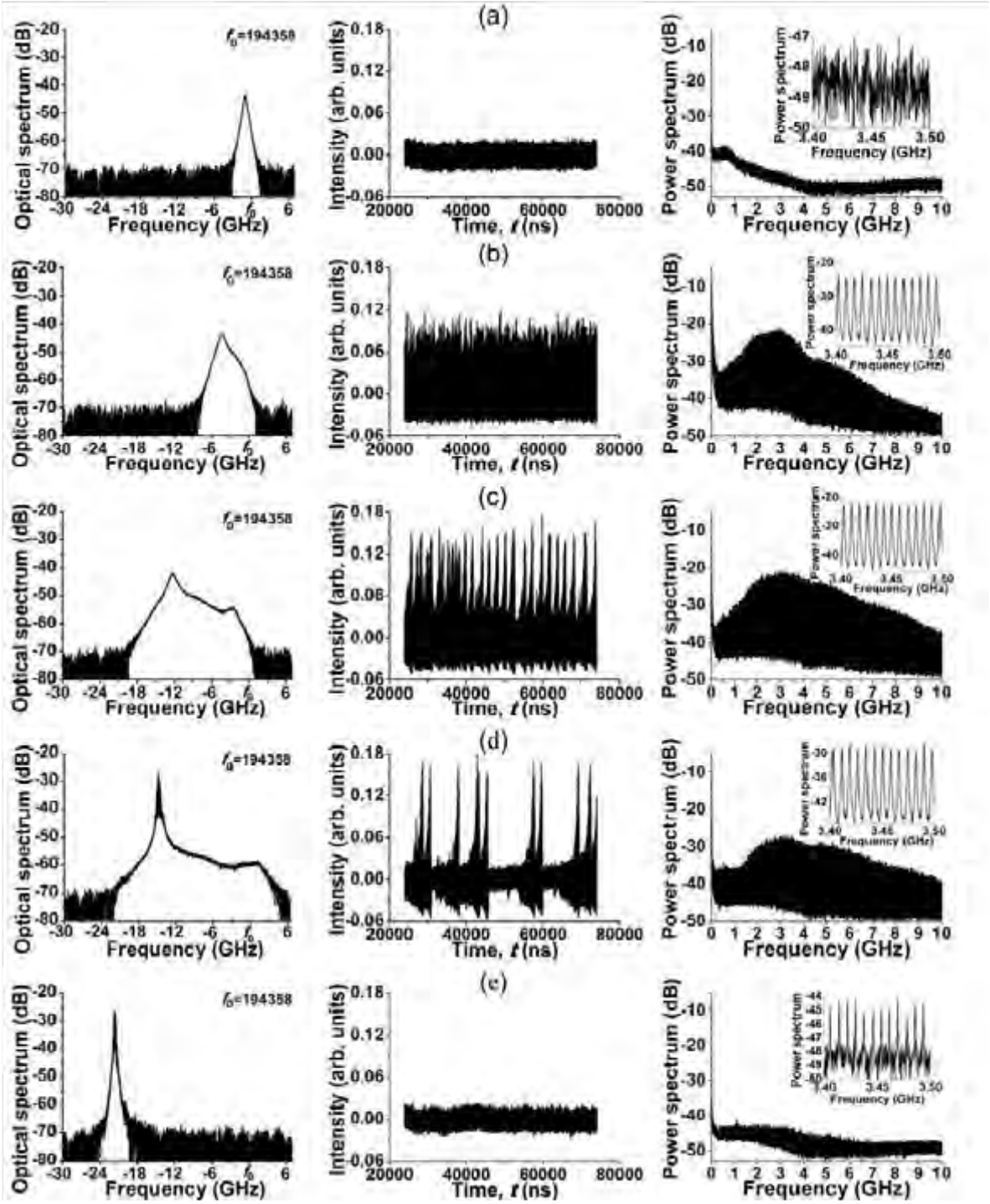

Figure 3.2. Optical spectra (left), time series (middle), and rf spectra (right) for different attenuation values: (a) -34 dB, (b) -24 dB, (c) -10 dB, (d) -2 dB, and (e) -2 dB (CW). The insets in the rf spectra show an enlargement around 3.45 GHz in order to visualize the frequency peaks corresponding to the interference between compound cavity modes.

3.4.2. Synchronization

The synchronization of two lasers can be characterized by the cross-correlation function [38]:

$$C(\Delta t) = \frac{\left\langle \left[I_1(t) - \langle I_1 \rangle \right] \left[I_2(t + \Delta t) - \langle I_2 \rangle \right] \right\rangle}{\left\{ \left\langle \left[I_1(t) - \langle I_1 \rangle \right]^2 \right\rangle \left\langle \left[I_2(t) - \langle I_2 \rangle \right]^2 \right\rangle \right\}^{1/2}} \quad , \tag{1}$$

where I_1 and I_2 are the output intensity of laser 1 and laser 2, respectively. Angle brackets < > denote time average, and Δt is the time shift. Figure 3.3 shows the time series (left), synchronization diagram (middle), and cross-correlation (right) between strongly coupled SLs (k = -4 dB) operating in the LFF regime. The synchronization diagram is constructed by plotting the intensity of laser 1 versus the intensity of laser 2 after compensating for the coupling time, this means that we shifted in time with respect to each other. It provides an indication of the synchronization quality, even though we refer to generalized synchronization here; a high degree of synchronization results in a diagram that orders around a 45-degree line. The two maxima in the cross-correlation function (right panel) occur at time lags equal to $\pm\tau_c$ = 63 ns. For k = -4 dB, the maximum cross-correlation coefficient is C_{max} = 0.83, indicating stable achronal synchronization.

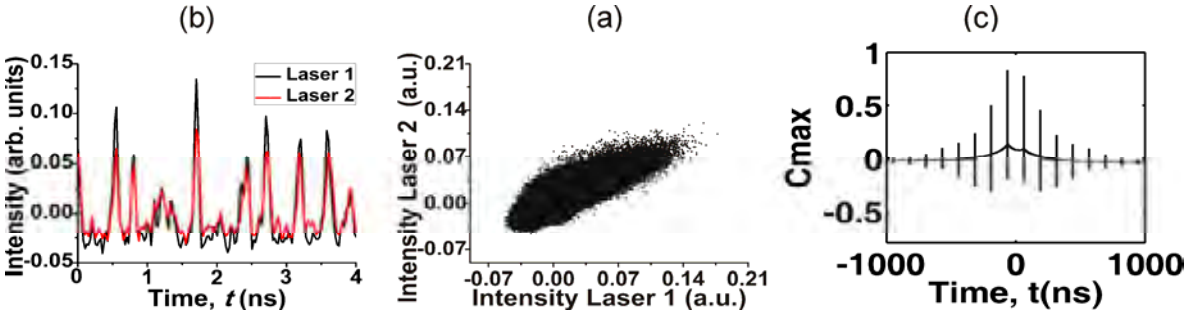

Figure 3.3. Time series (left), phase portraits (middle), and cross-correlations (right) between two lasers for k = -4 dB demonstrating achronal synchronization. The time lag is compensated in both the time series and phase portrait.

Figure 3.4 depicts the maximum of the cross-correlation coefficient and the average emitted power as functions of the attenuation. As the attenuation is decreased, C_{max} increases up to its maximum value of 0.83. Then, in the large coupling region, C_{max} drops to almost zero when the lasers switch to a noisy stable steady state of the compound cavity. The average emitted power increases with an increasing attenuation, even when the lasers are in the bistable regime.

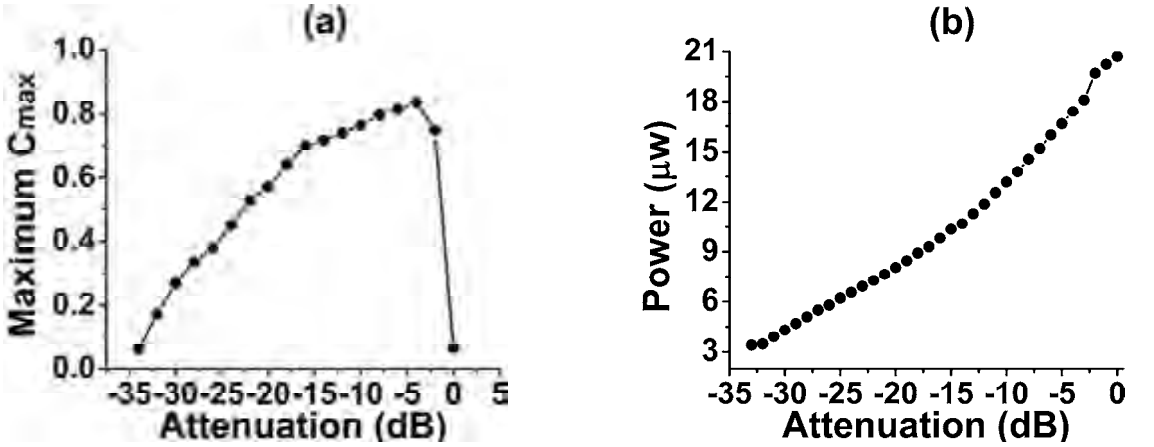

Figure 3.4. (a) Maximum cross-correlation C_{max} between lasers and (b) average power of one of the lasers as functions of attenuation.

3.5. Laser behaviour for $I = 1.25\ I_{th}$

In this section, we study the laser dynamics and synchronization properties of the mutually coupled SLs when the bias current is set at $I = 1.25\ I_{th}$.

3.5.1. Intensity dynamics, optical and rf spectra

The laser' temporal and spectral dynamics are different from that observed in the previous case of lower current ($I = 1.02\ I_{th}$). Figure 3.5 shows the optical spectra of the uncoupled lasers, which are almost identical. They exhibit the characteristics of single mode emission with relaxation oscillation sidebands.

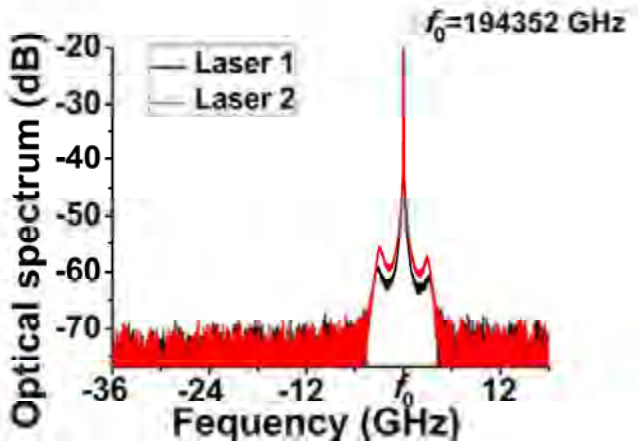

Figure 3.5. Optical spectra of solitary lasers.

The optical spectra for different attenuations are shown in Fig. 3.6. For the maximum value of attenuation (k = -36 dB) we can see in Fig. 3.6(a) that the lasers exhibit the characteristics of single mode emission with relaxation oscillation sidebands as the optical spectra of the uncoupled laser. When the attenuation is decreased, we observe undamped relaxation oscillations [Figs. 3.6 (b,c)] and a transition to chaotic emission with multiple compound cavity modes, resulting in the significant linewidth broadening [Figs. 3.6 (d,e)]. Similarly to the case of the low bias current, the spectrum shifts towards smaller frequencies (longer wavelengths) [Figs 3.6 (f,g)]. Interestingly, the optical spectrum for 0-dB attenuation [Fig. 3.5 (h)] shows two distinct spectral contributions, around the solitary laser frequency and the modes with higher optical gain, respectively.

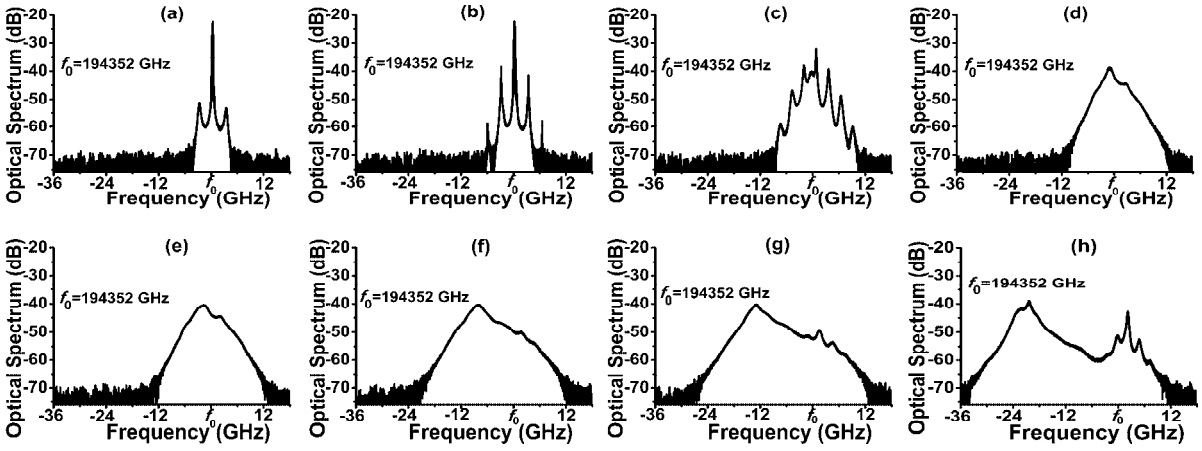

Figure 3.6. Optical spectra for different attenuation values: (a) -36 dB, (b) -34 dB, (c) -30 dB, (d) -24 dB, (e) -20 dB, (f) -10 dB, (g) -6 dB, and (h) 0 dB.

Figure 3.7 shows typical rf spectra for different attenuation values. The dominant frequencies are 2.77 GHz, 2.66 GHz, 2.81 GHz, and 2.3 GHz for -36 dB, -30 dB, -24 dB, and 0 dB, respectively. It can be seen that even for high attenuation, the lasers exhibit undamped relaxation oscillations [See Fig. 3.7 (a)]. For an attenuation of -30 dB we can see clearly that the frequencies spaced by ~7.9 MHz correspond to the interference between compound cavity modes, the contribution of these frequency peaks is significant and these peaks are distributed in a rather regular way [see the inset in Fig. 3.7 (b)]. For smaller attenuation (k = -24 dB) the power is more distributed along the different frequency components and the compound cavity peaks structure is more irregular [see the inset in Fig. 3.7 (c)].

The distribution of power over a wider frequency range is accompanied by the significant spectral broadening [Fig. 3.7 (c)] that suggests an increasing complexity (chaoticity) of the laser oscillations. For very low attenuation, the contribution of the compound cavity modes is very strong, thus further increasing the system complexity [Fig. 3.7 (d)].

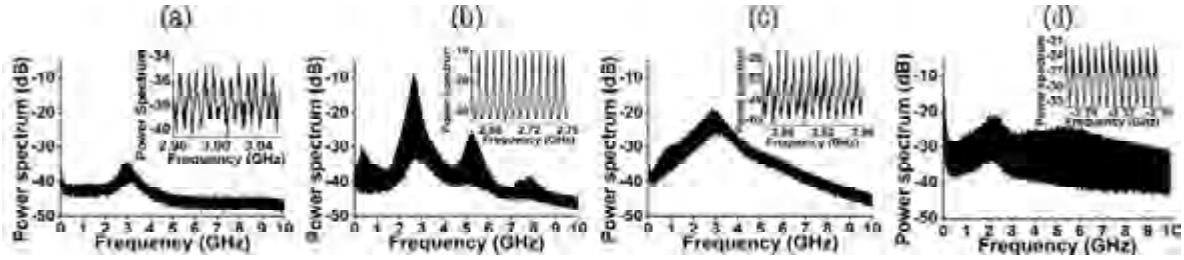

Figure 3.7. rf spectra for different attenuation (a) -36 dB, (b) -30 dB, (c) -24 dB, and (d) 0 dB. The insets show enlarged parts of the rf spectra close to the maxima.

3.5.2. Synchronization

Figure 3.8 shows the laser time series (left panels), the corresponding synchronization diagrams (middle panels), and the cross-correlation functions (right panels) for $I = 1.25\ I_{th}$. The lasers display different synchronization states for different attenuation values. For the maximum value of attenuation (k = -36 dB) the maximum cross-correlation is $C_{max} = 0.12$, indicating that the lasers oscillate very asynchronously [Figs. 3.8 (a)].

For high attenuation (between -36 dB and -30 dB), *intermittent achronal synchronization* is observed [Figs. 3.8 (b)]. In this regime the lasers are synchronized only in the windows of large-amplitude oscillations, whereas in the zones of low-amplitude oscillations the lasers oscillate asynchronously. The complex fine structure in the figure of the cross-correlation reflects this synchronization state. For an attenuation of -30 dB, the lasers become continuously synchronized and the cross-correlation reaches its maximum value (C_{max} = 0.82) [Figs. 3.9 (c)]. For this attenuation, *achronal synchronization* is observed with a pronounced maximum in the cross-correlation function.

For stronger coupling (k = -20 dB) [Figs. 3.8 (d)], the maximum of the cross-correlation decreases until $C_{max} = 0.21$, indicating that the synchronization is being lost. Finally, for the minimum attenuation value of 0 dB (maximum coupling), we observe stable achronal synchronization [Figs. 3.8 (e)]. Unlike the case of the bias current close to the threshold, for this higher current we do not observe bistability.

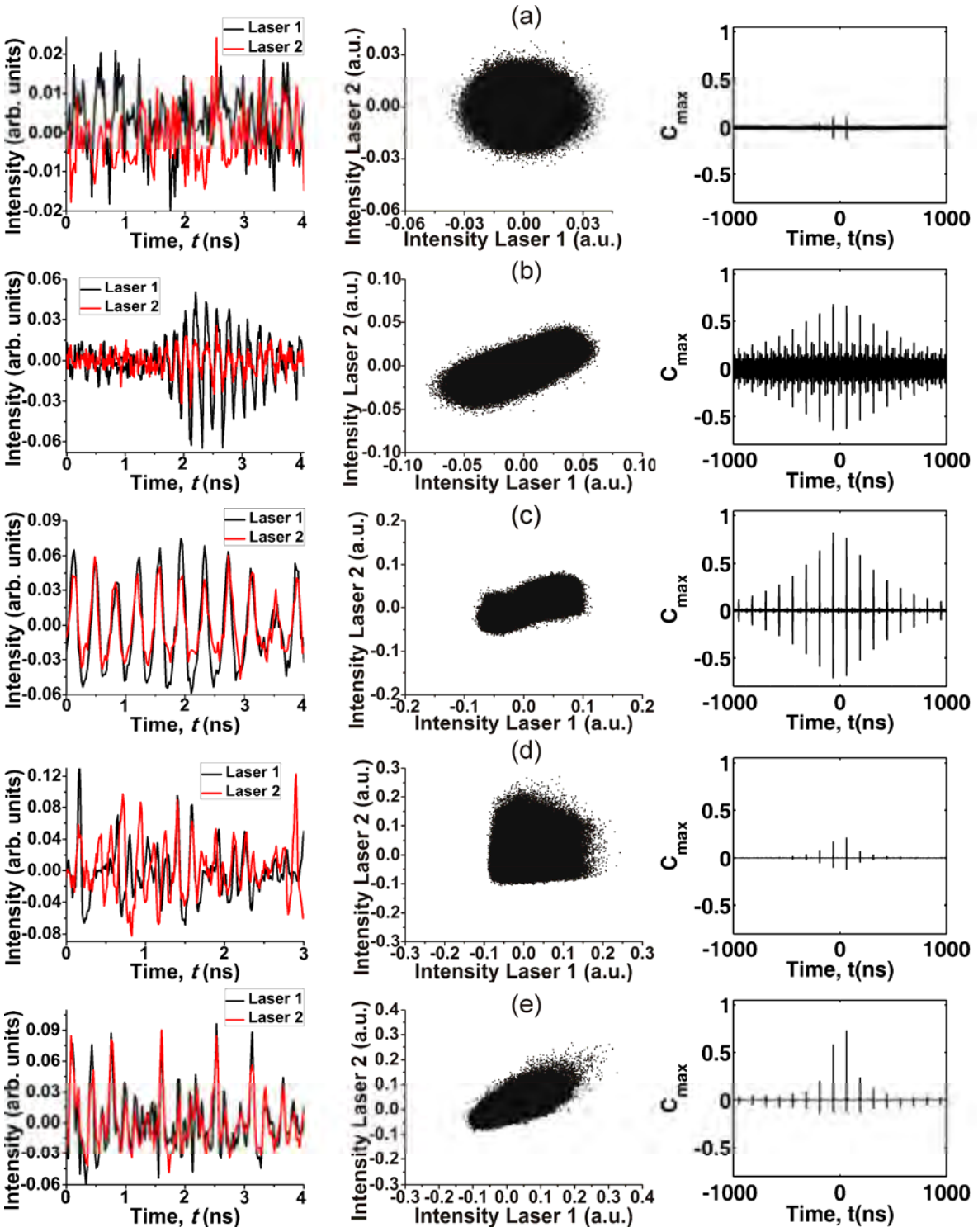

Figure 3.8. Time series of laser intensities (left) and synchronization diagrams with compensated coupling time (middle), and cross-correlation (right) for different attenuations: (a) -36 dB, (b) -34 dB, (c) -30 dB, (d) -20 dB, and (e) 0 dB.

In Figure 3.9, we plot the maximum cross-correlation and the average output power versus the attenuation. Interestingly, the maximum cross-correlation depends non-monotonously on the attenuation and four qualitatively different regions can be distinguished. As observed in the case of very low bias current, for the strongest attenuation the lasers oscillate asynchronously (see point *a* in Figure 3.9).

In the region ($\overline{ab}$), intermittent achronal synchronization is observed. As the attenuation is decreased, the average cross-correlation increases because the windows of synchronization become longer. For an attenuation of -30 dB (at point *b*), the lasers are all the time well synchronized. In the region ($\overline{bc}$), the cross-correlation decreases, i.e. synchronization degrades. This decrease in the cross-correlation is associated with the transition from weak to strong chaos recently reported in [39,40]. In the region ($\overline{cd}$), the maximum of the cross-correlation increases with decreasing attenuation, i.e., the almost uncorrelated state observed at point *c* gives rise to a highly-synchronized state (illustrated at point *d*). This increase in the cross-correlation is associated with the transition from strong back to weak chaos [39,40]. The high degree of synchronization remains up to the minimum attenuation, depicted as point *e*. The cross-correlation saturates around 0.75 and does not change in the region ($\overline{de}$). It is important to note that complete synchronization is never achieved. It can be seen in Fig. 3.9 (b) that the average power increases monotonously with decreasing attenuation as in the case for low bias current.

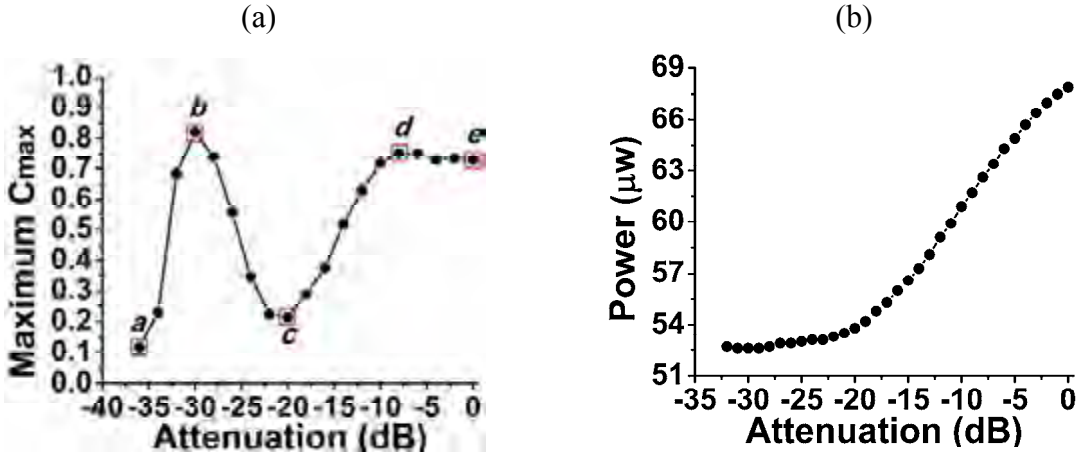

Figure 3.9. (a) Maximum cross-correlation between lasers and (b) average power of one of the lasers versus attenuation.

3.6. Discussion and conclusion

We have experimentally investigated the spectral and temporal characteristics of two mutually delay-coupled semiconductor lasers. By exploring the coupling strength dependence for two different values of the bias current: 1.02 and 1.25 times the threshold bias current of the solitary laser, we have found different dynamical regimes and different synchronization states. For the low injection current (I = 1.02 I_{th}), we observed that the maxima of the cross-correlation function increased with decreasing attenuation between the lasers. For low attenuation (strong coupling), we found the coexistence of LFF and CW regimes; these two regimes alternated in time due to spontaneous emission and carrier noise. Although the coupled lasers exhibited stable emission, their optical spectra were different from those of the solitary lasers; the central frequency of the coupled lasers was shifted towards lower frequencies, corresponding to the stable high gain compound cavity modes. The average power of the lasers increased as the attenuation was decreased, independently of the changes in the dynamical regime.

The dynamics was more complex when the lasers were operated at higher bias currents (I = 1.25 I_{th}). A transition to chaotic emission with multiple compound cavity modes and a significant linewidth broadening were observed when the attenuation was decreased. Different synchronization states were identified for different attenuation values. Interestingly, the maximum cross-correlation between the lasers' intensities changed non-monotonously as the attenuation factor was decreased. For low couplings the cross-correlation increased from 0.12 to 0.82; it decreased to 0.21 for intermediate coupling values and then again increased until it saturates to about 0.75 for large couplings. The qualitative changes in this dependence were associated with changes in the dynamical regimes. Correlation degraded in the strong chaos dynamical regime, while the maximum correlation was larger in the weak chaos regions. However, we did not find significant differences in the maximum values of cross-correlation for strongly coupled lasers, when the laser was pumped at the 1.02- and 1.25- threshold currents. In both cases stable achronal synchronization was observed. Regarding synchronization, the weakly coupled lasers were intermittently synchronized in time. The lasers were synchronized only in those

temporal windows with large-amplitude spikes, while they oscillated asynchronously in windows with low-amplitude spikes. For smaller attenuations, the lasers were continuously synchronized but, due to the increasing complexity of the coupled system, they lost synchronization. For strong coupling (very low attenuation, 0dB to -12 dB) they synchronized again in the generalized achronal synchronization state. Unlike the case of low bias current, for higher bias current we did not observe bistability between chaotic pulsations and CW emission.

3.7. References

1. J. R. Leger, M. L. Scott, and W. B. Veldkamp, Appl. Phys. Lett., vol. 52, (1988), 1771-1773.
2. E. C. Serrat, M. C. Torrent, J. García-Ojalvo, and R. Villaseca, Phys. Rev. A, vol. 64 (2001), 0418021-4.
3. S. Donati and C. R. Mirasso, IEEE J. Quantum Electron., vol. 38 (2002), 1138-1204.
4. A. Argyris, D. Syvridis, L. Larger, V. Annovazzi-Lodi, P. Colet, I. Fischer, J. García-Ojalvo, C. R. Mirasso, L. Pesquera and K. A. Shore, Nature, vol. 438 (2005), 343-346.
5. A. Uchida, K. Amano, M. Inoue, K. Hirano, S. Naito, H. Someya, I. Oowada, T. Kurashige, M. Shiki, S. Yoshimori, K. Yoshimura, and P. Davis, Nature Photonics, vol. 2 (2008), 728-732.
6. I. Reidler, Y. Aviad, M. Rosenbluh, and I. Kanter, Phys. Rev. Lett., vol. 103 (2009), 241021-4.
7. N. Oliver, M. C. Soriano, D. W. Sukow, and I. Fischer, Opt. Lett., vol. 36 (2011), 4632-4634.
8. D. Brunner, M. C. Soriano, C. R. Mirasso, and I. Fischer, Nature Comm., vol. 4 (2013), 1364-1367.

9. M.C. Soriano, J. Garcia-Ojalvo, C.R. Mirasso, I. Fischer, Reviews of modern physics vol. 85 (2013), 421-425.
10. T. Heil, I. Fischer, W. Elsäßer, J. Mulet, and C. R. Mirasso, Phys. Rev. Lett., vol. 86 (2001), pp. 795-798.
11. H. Fujino and J. Ohtsubo, Opt. Rev., vol. 8 (2001), 351-357.
12. T. Heil, I. Fischer, and W. Elsäßer, Phys. Rev. A, vol. 58 (1998), R2672-R2675.
13. G. H. M. van Tartwijk and D. Lenstra, Quantum Semiclass. Opt., vol. 7 (1995), 87-143.
14. T. Heil, I. Fischer, and W. Elsäßer, Phys. Rev. A, vol. 60 (1999), 634-641.
15. V. Ahlers, U. Parlitz, and W. Lauterborn, Phys. Rev. E, vol. 58 (1998), 7208-7213.
16. C. Masoller, Phys. Rev. Lett., vol. 86 (2001), 2782-2785.
17. I. Wedekind and U. Parlitz, Int. J. Bifurc. Chaos, vol. 11 (2001), 1141-1147.
18. J. M. Buldú, R. Vicente, T. Pérez, C. R. Mirasso, M. C. Torrent, and J. García- Ojalvo, Appl. Phys. Lett., vol. 81 (2002), 5105-5107.
19. J. Mulet, C. Mirasso, T. Heil, and I. Fischer, J. Opt. B: Quantum Semiclass. Opt., vol. 6 (2004), 97-105.
20. H. Erzgräber, D. Lenstra, and B. Krauskopf, Opt. Comm., vol. 255 (2005), 286- 296.
21. A. Hohl, A. Gavrielides, T. Erneux, and V. Kovanis, Phys. Rev. Lett., vol. 78 (1997), 4745-4748.
22. A. Hohl, A. Gavrielides, T. Erneux, and V. Kovanis, Phys. Rev. A, vol. 59 (1999), 3941-3949.
23. N. Gross, W. Kinzel, I. Kanter, M. Rosenbluh, and L. Khaykovich, Opt. Comm., vol. 267 (2006), 464-468.

24. J. K. White, M. Matus, J. V. Moloney, Phys. Rev. E, vol. 65 (2002), 0362291-5.

25. E. Klein, N. Gross, M. Rosenbluh, W. Kinzel, L. Khaykovich, and I. Kanter, Phys. Rev. E, vol. 73 (2006), 0662141-4.

26. E. A. Viktorov, A. M. Yacomotti, and P. Mandel, J. Opt. B: Quantum Semiclass. Opt., vol. 6 (2004), L9-L12.

27. I. Fischer, V. Raul, J. Buldú, M. Peil, C. Mirasso, M. Torrent, and J. García-Ojalvo, Phys. Rev. Lett., vol. 97 (2006), 123902-123905.

28. R. Vicente, C. R. Mirasso, and I. Fischer, Opt. Lett., 32 (2007), 403-405.

29. F. Rogister and M. Blondel, Opt. Comm., vol. 239 (2004), 173-180.

30. T. Deng, G. Xia, Z. Wu, X. Lin, and J. Wu, Opt. Express, vol. 19 (2011), 8762-8773.

31. R. W. Tkach and A. R. Chraplyvy, J. Lightwave Technol., Vol. LT-4 (1986), 1655-1661.

32. L. Goldberg, H. F. Taylor, A. Dandridge, J. F. Weller, and R. O. Miles, IEEE J. Quantum Electron., vol. QE-18 (1982), 555-563.

33. G. A. Acket, D. Lenstra, A. J. Den Boef, and B. H. Verbeek, IEEE J. Quantum Electron., vol. QE-20 (1984), 1163-1169.

34. J. Mørk, B. Tromborg, and J. Mark, IEEE J. Quantum Electron. 28 (1992) 93-108.

35. G. Van der Sande, M. C. Soriano, I. Fischer, and C. R. Mirasso, Phys. Rev. E, vol. 77 (2008), 0552021-4.

36. J. Mørk, B. Tromborg, and P. L. Christiansen, IEEE J. Quantum Electron., vol. QE-24 (1988), 123-131.

37. J. Wang and K. Petermann, IEEE J. Quantum Electron., vol. QE-27 (1991), 3-9.

38. M.C. Soriano, F. Ruiz-Oliveras, P. Colet, and C. R. Mirasso, Phys. Rev. E, vol. 78 (2008), 0462181-5.

39. S. Heiligenthal, T. Dahms, S. Yanchuk, T. Jüngling, V. Flunkert, I. Kanter, E. Schöll, and Wolfgang Kinzel, Phys. Rev. Lett., vol. 107 (2011), 2341021-5.

40. S. Heiligenthal, T. Jüngling, D. A. Arroyo-Almanza, O. D'Huys, M. C. Soriano, I. Fischer, I. Kanter, and W. Kinzel, arXiv:1210.1887.

Chapter 4. Route to chaos in a ring of three unidirectionally coupled semiconductor lasers

---

"Only two things are infinite, the universe and human stupidity, and I am not sure about the former."

Albert Einstein

4.1. Abstract

Complex dynamics of a ring of three unidirectionally-coupled semiconductor lasers are studied with respect to the coupling strength. While uncoupled, the lasers stay in a continuous-wave regime; they begin to oscillate as the coupling strength reaches a certain threshold value. When the coupling further increases, the dynamics exhibit a route to chaos via a sequence of Hopf bifurcations resulting in periodic, quasiperiodic, and chaotic oscillations. In the chaotic range, different synchronization states, ranging from asynchronous behavior to phase and near synchronization, are observed. The analytical solution yields a large number of fixed points.

4.2 Introduction

Semiconductor lasers (SLs) with optical injection or delayed feedback have been widely studied due to their potential applications in secure communications [1]–[3]. Recent research on coupled SLs has examined various mechanisms for their synchronization that may be useful to design optical communication networks [1]–[6]. To reveal dynamical properties of optical networks, it is very important first to understand the features of basic building blocks, such as rings or chains. Several works demonstrate that delay in coupling results in complex dynamical behavior in otherwise continuous wave lasers [5], [6]. Three SLs coupled unidirectionally in a closed chain exhibit a large correlation between chaotic oscillations for a strong coupling strength [7]. Ring can be deduced from the correlation of a single oscillator with delayed feedback, where the autocorrelation decays exponentially [8]. Recently, a ring of three bidirectionally coupled SLs was proposed for secure optical communication based on chaos synchronization [9]. However, isochronal synchrony of bidirectionally delay-coupled systems is not so stable as achronal synchrony of unidirectionally coupled systems [6]. The delays in coupling interaction can be ignored in unidirectional systems, thus posing a fundamental challenge to synchronization.

In all previous studies, a fixed value for the coupling strength was explored; no work to our knowledge was done to study the dependence of the laser ring dynamics on the coupling strength. In this Letter, we address the questions: What route to chaos will a ring of lasers exhibit while the coupling strength is increasing? and How will the lasers be synchronized on this route? The answers to these questions will provide a new step towards understanding of the collective behavior of coupled SLs to select adequate laser parameters and configuration for optimal network performance.

4.3 Model

The configuration of our system is schematically drawn in Fig. 4.1. This system consists in three semiconductor lasers unidirectional coupled in a ring configuration. The output beam of the first semiconductor laser is introduced to the second laser and so on.

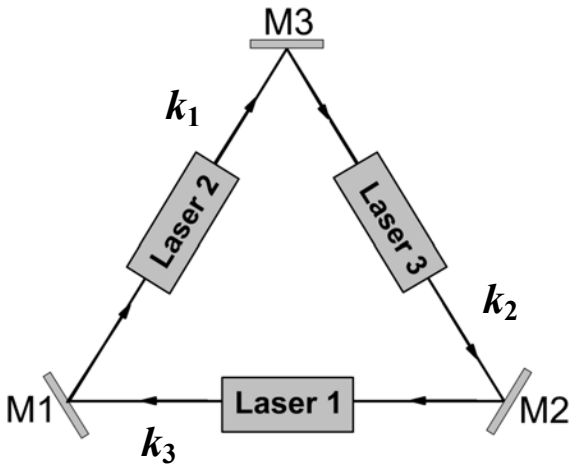

Figure 4.1. Three semiconductor lasers unidirectional coupled in a ring configuration, where k_1, k_2 and k_3 represent the strength of coupling received by laser m. M_1, M_2 and M_3 represent mirrors

The model equations to describe the dynamics of a ring of SLs can be derived from the Lang-Kobayashi equations [10] for the complex electric field $E = Ex + iE_y$, and the carrier number N, written as [11], [12]

For Laser 1:

$$\dot{E}_1(t) = \frac{1}{2}(1+i\alpha)\left[g\left(N_1(t)-N_0\right)-\gamma_p\right]E_1(t) + kE_3\left(t-\tau\right)e^{iC_{p1}} \tag{4.1}$$

$$\dot{N}_1(t) = \frac{I_1}{e} - \gamma_n N_1(t) - g\left(N_1(t)-N_0\right)\left|E_1(t)\right|^2 \tag{4.2}$$

For laser 2:

$$\dot{E}_2(t) = \frac{1}{2}(1+i\alpha)\left[g\left(N_2(t)-N_0\right)-\gamma_p\right]E_2(t) + kE_1\left(t-\tau\right)e^{iC_{p2}} \tag{4.3}$$

$$\dot{N}_2(t) = \frac{I_2}{e} - \gamma_n N_2(t) - g\left(N_2(t)-N_0\right)\left|E_2(t)\right|^2 \tag{4.4}$$

For laser 3:

$$\dot{E}_3(t) = \frac{1}{2}(1+i\alpha)\left[g\left(N_3(t)-N_0\right)-\gamma_p\right]E_3(t) + kE_2\left(t-\tau\right)e^{iC_{p3}} \tag{4.5}$$

$$\dot{N}_3(t) = \frac{I_3}{e} - \gamma_n N_3(t) - g\left(N_3(t)-N_0\right)\left|E_3(t)\right|^2 \tag{4.6}$$

where $g = 1.5 \times 10^{-5}$ ns^{-1} is the linear gain coefficient, $N_0 = 1.5 \times 10^8$ is the carrier number at transparency, $I_{1,2,3} = 2I_{th}$ is the electric pump current (I_{th} = 14.5 mA is the threshold current), e is the electron charge, $\gamma_e = 1/\tau_n$ (τ_n = 2 ns) is the carrier decay rate, $\alpha = 5$ is the linewidth enhancement factor, $\gamma_p = 1/\tau_p$ ($\tau_p = 2 \times 10^{-3}$ ns) is the photon decay rate, κ is the strength of injection received by laser m −1, τ = 3 ns is the coupling time between the lasers, that correspond to L = 0.9 cm, where L is the length between of lasers, and $C_{p1,2,3} = \omega_0\tau$ is the phase of the injected field ($\omega_0 = 1.2\times10^6$ ns^{-1} being the free-running optical frequency in radians). For simplicity, the laser parameters are considered to be the same for all lasers. $|E_{1,2,3}|^2 = I_{1,2,3}$ is the normalized optical intensity. For the fixed point analysis, we rewrite equation (4.1) to (4.6) in the polar coordinates substituting $E_{1,2,3}(t)$ by

$$E_{1,2,3}(t) = R_{1,2,3}(t)e^{i\phi_{1,2,3}(t)} \tag{4.7}$$

To obtain the following equations for the three semiconductor lasers [12],

For laser 1 are:

$$\dot{R}_1(t) = \frac{1}{2}\left[g\left(N_1(t) - N_0\right) - \gamma_p\right]R_1(t) + kR_3(t-\tau)\cos\left[\phi_3(t-\tau) - \phi_1(t) - C_{p1}\right], \tag{4.8}$$

$$\dot{\phi}_1(t) = \frac{\alpha}{2}\left[g\left(N_1(t) - N_0\right) - \gamma_p\right] + k\frac{R_3(t-\tau)}{R_1(t)}\sin\left[\phi_3(t-\tau) - \phi_1(t) - C_{p1}\right], \tag{4.9}$$

$$\dot{N}_1(t) = \frac{I_1}{e} - \gamma_e N_1(t) - g\left(N_1(t) - N_0\right)R_1^2(t). \tag{4.10}$$

For laser 2 are:

$$\dot{R}_2(t) = \frac{1}{2}\left[g\left(N_2(t) - N_0\right) - \gamma_p\right]R_2(t) + kR_1(t-\tau)\cos\left[\phi_1(t-\tau) - \phi_2(t) - C_{p2}\right], \tag{4.11}$$

$$\dot{\phi}_2(t) = \frac{\alpha}{2}\left[g\left(N_2(t) - N_0\right) - \gamma_p\right] + k\frac{R_1(t-\tau)}{R_2(t)}\sin\left[\phi_1(t-\tau) - \phi_2(t) - C_{p2}\right], \tag{4.12}$$

$$\dot{N}_2(t) = \frac{I_2}{e} - \gamma_e N_2(t) - g\left(N_2(t) - N_0\right)R_2^2(t). \tag{4.13}$$

For laser 3 are:

$$\dot{R}_3(t) = \frac{1}{2}\left[g\left(N_3(t) - N_0\right) - \gamma_p\right]R_1(t) + kR_2(t-\tau)\cos\left[\phi_2(t-\tau) - \phi_3(t) - C_{p3}\right], \quad [4.14]$$

$$\dot{\phi}_3(t) = \frac{\alpha}{2}\left[g\left(N_3(t) - N_0\right) - \gamma_p\right] + k\frac{R_2(t-\tau)}{R_3(t)}\sin\left[\phi_2(t-\tau) - \phi_3(t) - C_{p3}\right], \quad [4.15]$$

$$\dot{N}_3(t) = \frac{I_3}{e} - \gamma_e N_3(t) - g\left(N_3(t) - N_0\right)(t)R_3^2(t). \quad [4.16]$$

The solutions of (4.8), to (4.16) can be written as

$$R_{1,2,3}(t) = A_{s1,2,3}e^{i\omega_{s1,2,3}\tau} \quad , \quad N_m(t) = N_{s1,2,3} \quad [4.17]$$

where $A_{s1,2,3}$, $\omega_{s1,2,3}$, and $N_{s1,2,3}$ are constants. $\omega_{s1,23}\tau$ is the phase difference due to the distance between lasers 1 and 3, 2 and 1 and finally laser 3 and 2

$$\omega_{s1}\tau = \phi_1(t) - \phi_3(t-\tau) \quad [4.18]$$

$$\omega_{s2}\tau = \phi_2(t) - \phi_3(t-\tau) \quad [4.19]$$

$$\omega_{s3}\tau = \phi_3(t) - \phi_2(t-\tau) \quad [4.20]$$

The fixed points represent modes between two adjacent lasers. Inserting (4.17) into equations (4.8) to (4.16), we obtain

Laser 1:

$$0 = \frac{1}{2}\left[g\left(N_{s1}(t) - N_0\right) - \gamma_p\right]A_{s1} + kA_{s3}\cos\left(\omega_{s1}\tau + C_{p1}\right) \quad [4.21]$$

$$\omega_{s1} = \frac{\alpha}{2}\left[g\left(N_{s1}(t) - N_0\right) - \gamma_p\right] - k\frac{A_{s3}}{A_{s1}}\sin\left(\omega_{s1}\tau\right) + C_{p1} \quad [4.22]$$

$$0 = \frac{I_1}{e} - \gamma_e N_{s1} - \left[g\left(N_{s1}(t) - N_0\right) - \gamma_p\right]A_{s1}^2 \quad [4.23]$$

Laser 2:

$$0 = \frac{1}{2}\left[g\left(N_{s2}(t) - N_0\right) - \gamma_p\right]A_{s2} + kA_{s1}\cos\left(\omega_{s2}\tau + C_{p2}\right) \quad [4.24]$$

$$\omega_{s2} = \frac{\alpha}{2}\left[g\left(N_{s2}(t) - N_0\right) - \gamma_p\right] - k\frac{A_{s1}}{A_{s2}}\sin\left(\omega_{s2}\tau\right) + C_{p2} \quad [4.25]$$

$$0 = \frac{I_2}{e} - \gamma_e N_{s2} - \left[g\left(N_{s2}(t) - N_0\right) - \gamma_p\right]A_{s2}^2 \quad [4.26]$$

Laser 3:

$$0 = \frac{1}{2}\left[g\left(N_{s3}(t) - N_0\right) - \gamma_p\right]A_{s3} + kA_{s2}\cos\left(\omega_{s3}\tau + C_{p3}\right) \quad [4.27]$$

$$\omega_{s3} = \frac{\alpha}{2}\left[g\left(N_{s3}(t) - N_0\right) - \gamma_p\right] - k\frac{A_{s2}}{A_{s3}}\sin\left(\omega_{s3}\tau\right) + C_{p3} \quad [4.28]$$

$$0 = \frac{I_3}{e} - \gamma_e N_{s3} - \left[g\left(N_{s3}(t) - N_0\right) - \gamma_p\right]A_{s3}^2 \quad [4.29]$$

To solve for $N_{s1,2,3}$ in equations (4.21), (4.24), and (4.27) is transformed into

$$N_{s1} = \frac{-2kA_{s3}}{gA_1}\cos\left(\omega_{s1}\tau + C_{p1}\right) + N_0 + \frac{\gamma_p}{g} \quad [4.30]$$

$$N_{s2} = \frac{-2kA_{s1}}{gA_2}\cos\left(\omega_{s2}\tau + C_{p2}\right) + N_0 + \frac{\gamma_p}{g} \quad [4.31]$$

$$N_{s3} = \frac{-2kA_{s2}}{gA_3}\cos\left(\omega_{s3}\tau + C_{p3}\right) + N_0 + \frac{\gamma_p}{g} \quad [4.32]$$

Inserting equations (4.30), (4.31) and (4.32) into equations (4.22), (4.25) and (4.28) respectively, we get

$$\omega_{s1} = -k\frac{A_{s3}}{A_{s1}}\left[\alpha\cos\left(\omega_{s1}\tau + C_{p1}\right) + \sin\left(\omega_{s1}\tau + C_{p1}\right)\right] \quad [4.33]$$

$$\omega_{s2} = -k\frac{A_{s1}}{A_{s2}}\left[\alpha\cos\left(\omega_{s2}\tau + C_{p2}\right) + \sin\left(\omega_{s2}\tau + C_{p2}\right)\right] \quad [4.34]$$

$$\omega_{s3} = -k\frac{A_{s2}}{R_{s3}}\left[\alpha\cos\left(\omega_{s3}\tau + C_{p3}\right) + \sin\left(\omega_{s3}\tau + C_{p3}\right)\right] \quad [4.35]$$

The intensity can be calculated from equations (4.23), (4.26), and (4.29) as

$$A_{s1}^2 = \frac{\frac{I}{e} - \gamma_e N_{s1}}{g\left(N_{s1} - N_0\right)} \quad [4.36]$$

$$A_{s2}^2 = \frac{\frac{I}{e} - \gamma_e N_{s2}}{g\left(N_{s2} - N_0\right)} \quad [4.37]$$

$$A_{s3}^2 = \frac{\frac{I}{e} - \gamma_e N_{s3}}{g\left(N_{s3} - N_0\right)} \quad [4.38]$$

Now, assuming that all lasers are identical, we can state that the amplitudes of the electric fields are equal A_{s1}=A_{s2}=A_{s3}, thus equations (4.30) to (4.35) can be rewritten as the following pair of transcendental equations

Laser 1:

$$N_{s1} = -\frac{2k}{g}\cos\left(\omega_{s1}\tau + C_{p1}\right) + N_0 + \frac{\gamma_p}{g} \quad [4.39]$$

$$\omega_{s1} = -k\left[\alpha\cos\left(\omega_{s1}\tau + C_{p1}\right) + \sin\left(\omega_{s1}\tau + C_{p1}\right)\right] \quad [4.40]$$

Laser 2:

$$N_{s2} = -\frac{2k}{g}\cos\left(\omega_{s2}\tau + C_{p2}\right) + N_0 + \frac{\gamma_p}{g} \qquad [4.41]$$

$$\omega_{s2} = -k\left[\alpha\cos\left(\omega_{s2}\tau + C_{p2}\right) + \sin\left(\omega_{s2}\tau + C_{p2}\right)\right] \qquad [4.42]$$

Laser 3:

$$N_{s3} = -\frac{2k}{g}\cos\left(\omega_{s3}\tau + C_{p3}\right) + N_0 + \frac{\gamma_p}{g} \qquad [4.43]$$

$$\omega_{s3} = -k\left[\alpha\cos\left(\omega_{s3}\tau + C_{p3}\right) + \sin\left(\omega_{s3}\tau + C_{p3}\right)\right] \qquad [4.44]$$

4.4. Results of a ring of three unidirectionally-coupled semiconductor lasers.

The intersection of these three pairs of transcendental equations (equations (4.39) to (4.44)) defines a set of fixed points ($\omega_{s1,2,3}\tau$, $N_{s1,2,3}$) for a given effective coupling strength κ and phase $C_{p1,2,3}$.

Starting from zero coupling strength, where only one stable fixed point exists, the number of fixed points increases in pairs when the coupling strength κ is increased; each pair of fixed points is created in a saddle-node bifurcation. Figure 4.2 shows the fixed points and the chaotic trajectory projection of one of the lasers.

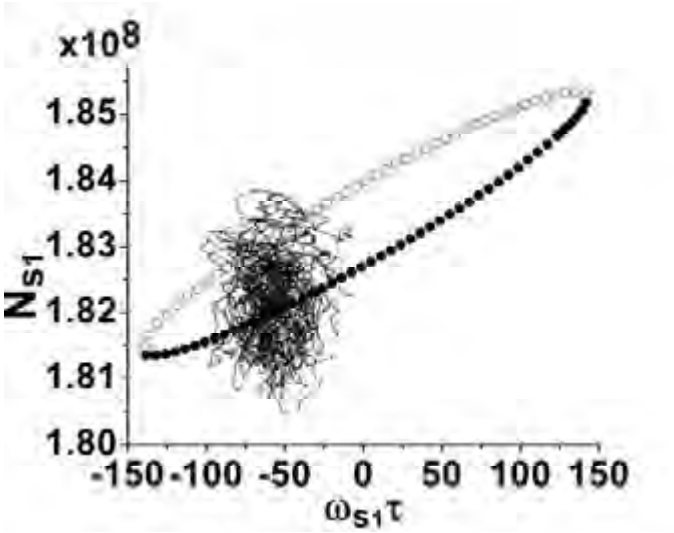

Figure 4.2. Fixed points (dots) and chaotic trajectory projection (curve) on ($\omega_{s1,2,3}\tau$, $N_{s1,2.3}$) space of one of the semiconductor laser in the ring for κ = 15 ns^{-1} and $C_{p1,2,3}$ = 0. The solid and open dots indicate modes and anti-modes, respectively.

Numerical simulations of (1), (2), and (3) are performed using a fourth order Runge-Kutta algorithm. Figures 4.3 (a-d) show the laser time series for different κ (231.44 ns^{-1} corresponds to a 100% coupling [13], i.e. if the total power is injected). When the coupling strength is small the lasers oscillate periodically [Fig. 4.3 (a) and (b)], for larger coupling quasiperiodicity takes place [Fig. 4.3 (c)], and at high coupling the lasers are chaotic [Fig. 4.3 (d)]. Figures 4.3 (e-h) display the corresponding power spectra with dominant frequencies 5.75 (e), 5.33 (f) and 5.64 GHz (g) for the periodic and quasiperiodic regimes. These frequencies are close to the relaxation oscillation frequency (5.6 GHz) of a solitary laser.

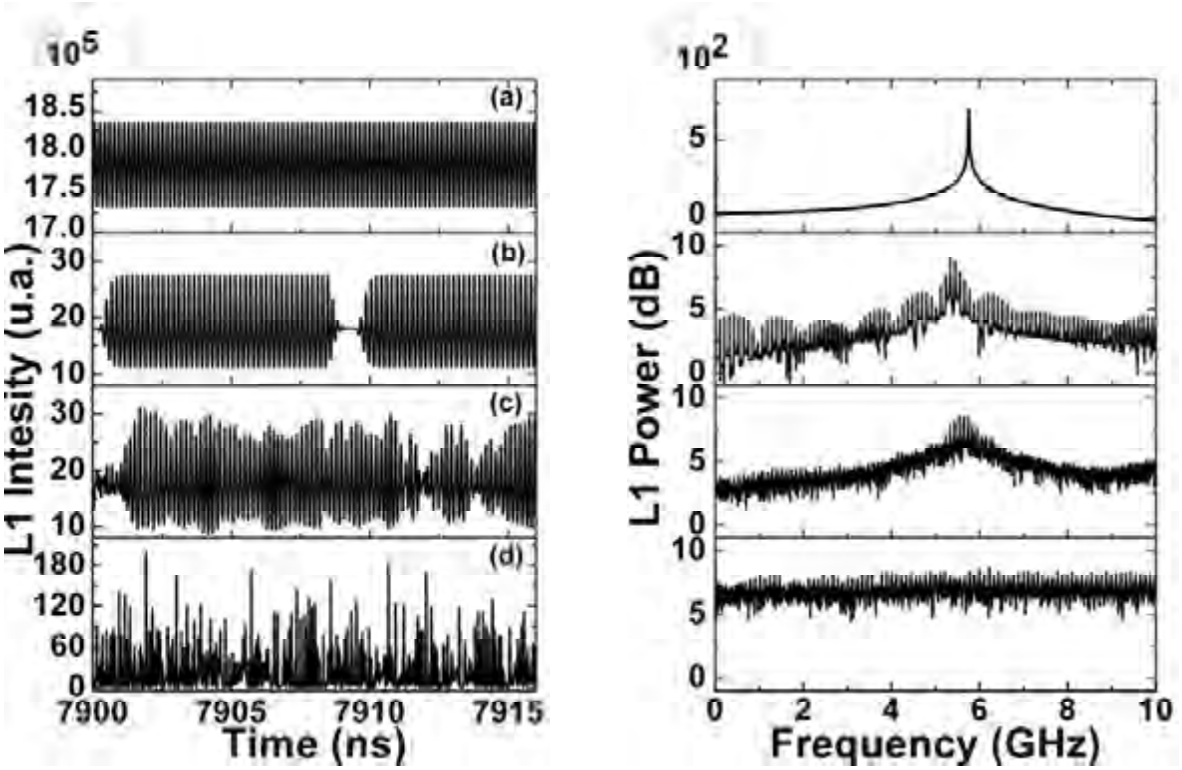

Figura 4.3. (a)–(d) Time series and (e)–(h) corresponding power spectra for (a) and (e) κ = 1.26 ns^{-1} (periodic regime), (b) and (f) κ = 2.6 ns^{-1} (frequency locking), (c) and (g) κ = 3.5 ns^{-1} (quasiperiodicity), and (d) and (h) κ = 100 ns^{-1} (chaos).

4.4.1 Bifurcation analyses

The bifurcation diagram in Fig. 4.4 (a) demonstrates the route to chaos via quasiperiodicity. To find a bifurcation point we use the method of branch tracing; while increasing adiabatically the coupling we take the final values of the variables as the initial conditions until the laser behavior changes. The quasiperiodic route to chaos was also observed in mutually coupled SLs [14]. Only two bifurcations are percussive to chaos, one standard Hopf bifurcation (HB) and one subsequent bifurcation to a two-frequency torus. When the third frequency is about to appear, a strange attractor simultaneously arises, since a three-frequency flow is destroyed by small perturbations. By means of three HBs, regular motion becomes highly unstable and is replaced by chaos.

In our system, a limit cycle with high frequency f_0 = 5.75 GHz arises in the first HB (H1) from the fixed point at κ = 1.26 ns^{-1}. A second HB (H2) gives rise a new frequency f_L = 0.105 GHz which is independent of κ, that creates a two-frequency torus [Fig. 4.3(b)]. The high frequency is locked by the low frequency and becomes $f_H = f_0 - nf_L$, where n = 0, 1, 2, 3, 4. Quotient f_H / f_L is always rational for $\kappa < 3.4$ ns^{-1} and in the torus bifurcation the motion becomes quasiperiodic. A further increase in κ results in another HB at $\kappa \approx 5$ ns^{-1} followed by the destruction of the torus and the emergence of a strange attractor, since the three-frequency flow is destroyed by small perturbations [15]. In both the periodic and quasiperiodic regions, the lasers are completely synchronized if the delay time is compensated. In the chaotic regime, the lasers lose synchronization, but with increasing κ their trajectories become more and more correlated [Fig. 4.4 (b)]. Although synchronization is improved, complete synchronization is never reached, even if the whole laser power is injected [16].

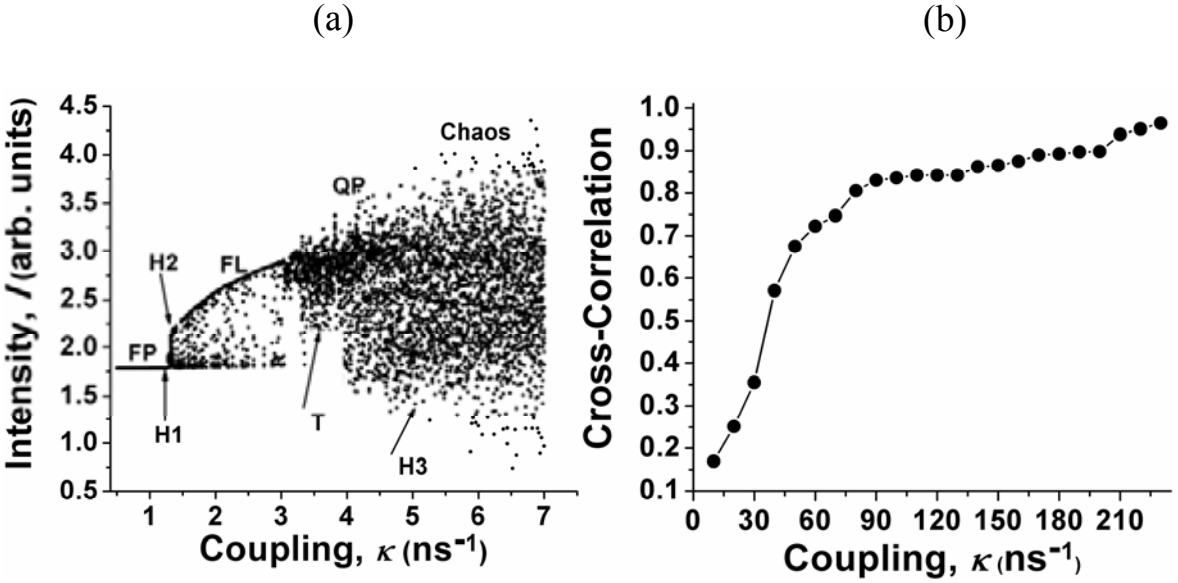

Figure 4.4. (a) Bifurcation diagram of peak-to-peak laser intensity and (b) cross-correlation between two lasers versus coupling strength. The laser being at low coupling in the fixed point (FP) undergoes a sequence of Hopf bifurcations (H1, H2, and H3) leading, respectively, to one-frequency periodic, two frequency locking (FL), and chaotic regimes. A torus bifurcation (T) results in quasiperiodicity (QP).

4.4.2. Synchronization analyses

Different synchronization states of the chaotic lasers were identified using commonly accepted criteria [17]. For $1 < \kappa < 3$ ns^{-1} the lasers oscillate in the periodic regimen and they have a complete synchronization [Fig. 4.5 (a, b)]. For $\kappa < 80$ ns^{-1} the lasers oscillate asynchronously [Figs. 4.5 (c, d)]; for 80 ns^{-1} $< \kappa <$ 200 ns^{-1} phase synchronization occurs [Fig. 4.5 (e, f)], and for higher κ the lasers become almost synchronized [Fig. 4.5 (g, h)] [7]. Since complete synchronization can never be reached for high coupling, the unidirectional coupling is not appropriate for secure communication.

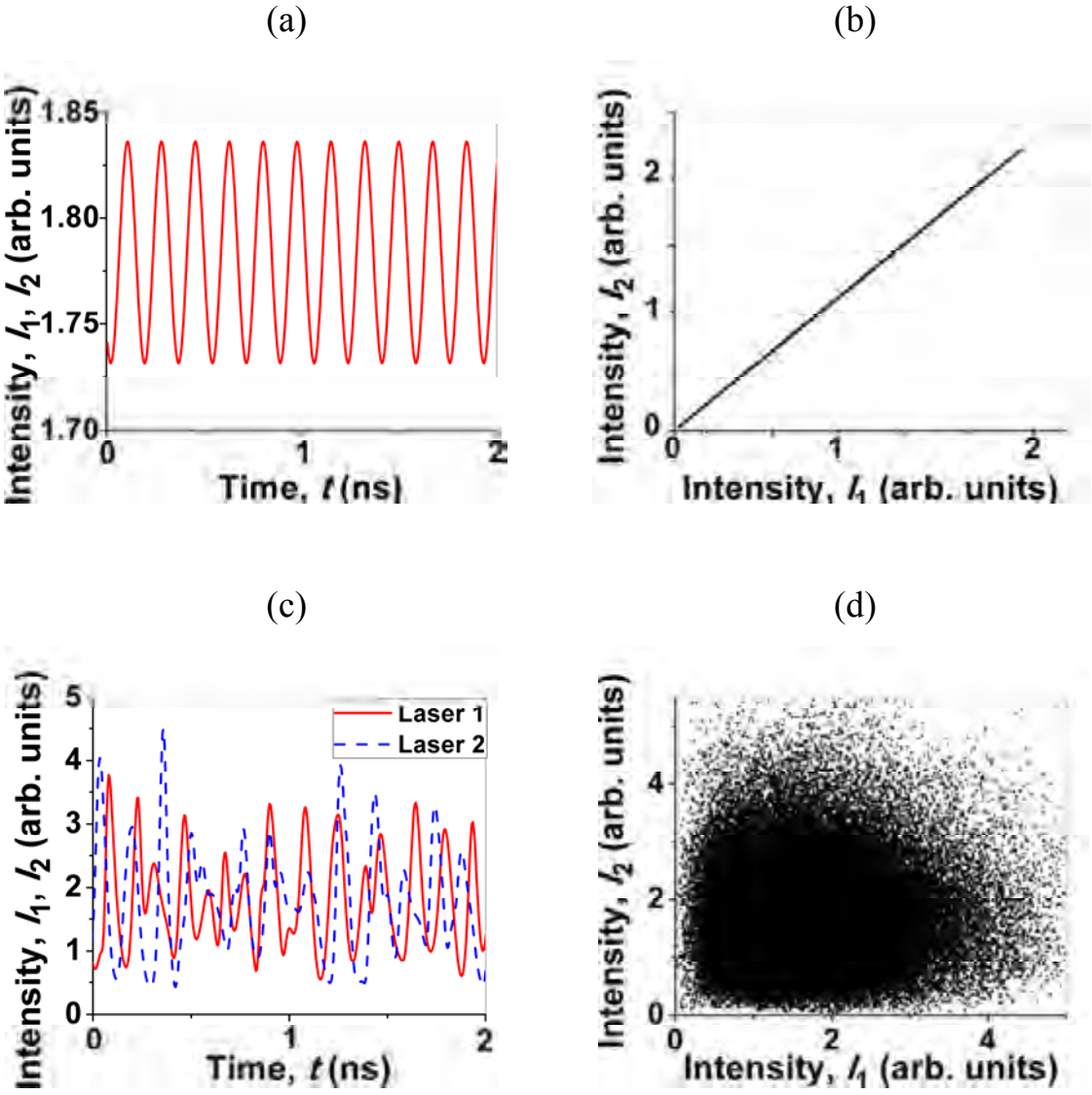

Figure 4.5 part A. (a) and (c) Time series and (b) and (d) corresponding phase space portraits of intensities of a pair of lasers. (a) and (b) complete synchronization for κ =1.26 ns^{-1}, (b) and (c) asynchronous motion for κ = 10 ns^{-1}. The delay time is compensated.

(e) (f)

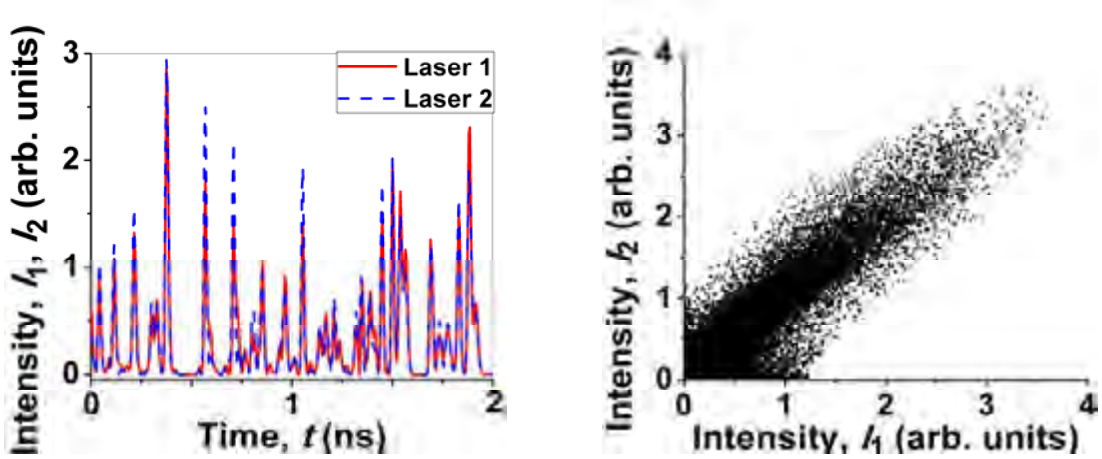

(g) (h)

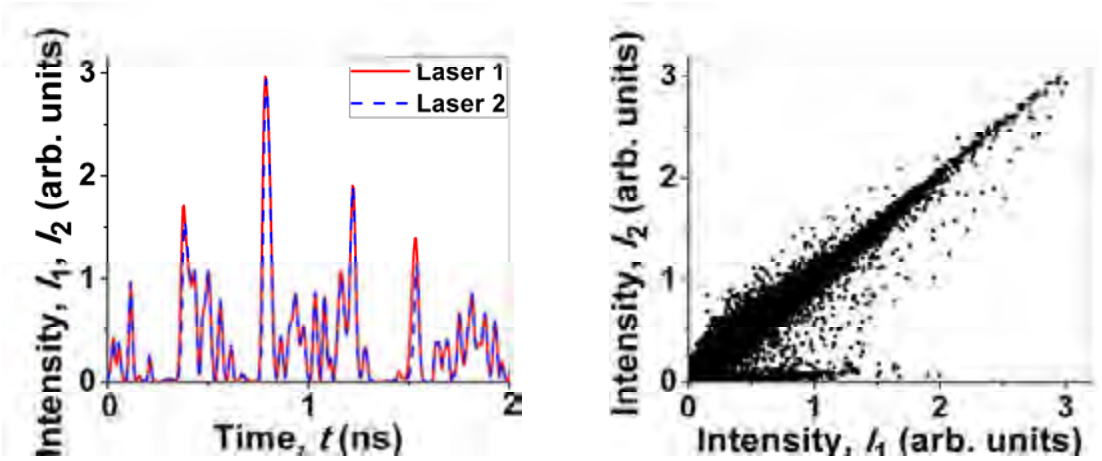

Figure 4.5. part B. (e) and (g) Time series and (f) and (h) corresponding phase space portraits of intensities of a pair of lasers. (e) and (f) phase synchronization for $\kappa = 160$ ns^{-1}. (g) and (h) almost synchronization for $\kappa = 230$ ns^{-1}. The delay time is compensated.

4.5. Conclusions

To conclude, we have shown that three SLs coupled unidirectionally in a ring exhibit a quasiperiodic route to chaos as the coupling strength is increased. While in the periodic and quasiperiodic regimes the lasers are completely synchronized (when the delay time is compensated), in the chaotic state they lose synchronization, and as the coupling is further increased, the lasers first become synchronized in phase and then almost synchronized. Although an increase in the coupling improves correlation, complete synchronization is never achieved even for 100% coupling. The results of this work may be useful for designing laser communication networks.

4.6 References

1. C. R. Mirasso, P. Colet, and P. García-Fernández, "Synchronization of chaotic semiconductor lasers: Application to encoded communications," IEEE Photon. Technol. Lett., vol. 8 (1996), 299–301.
2. A. Argyris, "Chaos-based communications at high bit rates using commercial fibre-optic links," Nature, vol. 438 (2005), 343–346.
3. A. N. Pisarchik and F. R. Ruiz-Oliveras, "Optical chaotic communication using generalized and complete synchronization," IEEE J. Quantum Electron., vol. (2010), 46279–284.
4. F. R. Ruiz-Oliveras and A. N. Pisarchik, "Phase-locking phenomenon in a semiconductor laser with external cavities," Opt. Express, vol. 14 (2006), 12859–12867.
5. F. R. Ruiz-Oliveras and A. N. Pisarchik, "Synchronization of semiconductor lasers with coexisting attractors," Phys. Rev. E, vol. 79 (2009), 0162021–8.

6. T. Heil, I. Fischer, W. Elsasser, J. Mulet, and C. Mirasso, “Chaos synchronization and spontaneous symmetry-breaking in symmetrically delay-coupled semiconductor lasers,” Phys. Rev. Lett., vol. 86 (2001), 795–798.
7. J. M. Buldú, M. C. Torrent, and J. García-Ojalvo, “Synchronization in semiconductor laser rings,” J. Lightw. Technol., vol. 25 (2007), 1549–1554.
8. G. Van der Sande, M. C. Soriano, I. Fischer, and C. R. Mirasso, “Dynamics, correlation scaling, and synchronization behavior in rings of delay-coupled oscillators,” Phys. Rev. E, vol. 77 (2008), 055202R-1–055202R-4.
9. Z.-C. Gao, Z.-M. Wu, L.-P. Cao, and G.-Q. Xia, “Chaos synchronization of optoelectronic coupled semiconductor lasers ring,” Appl. Phys. B, vol. 97 (2009) 645–651.
10. R. Lang and K. Kobayashi, “External optical feedback effects on semiconductor injection laser properties,” IEEE J. Quantum Electron., vol. 16 (1980), 347–355.
11. T. Heil, I. Fisher, W. Elsasser, K. Green, B. Krauskopf, and A. Gavrielides, “Delay dynamics of semiconductor lasers with short external cavities: Bifurcation scenarios and mechanisms,” Phys. Rev. E, vol. 67 (2003), 0662141–11.
12. V. Rottschäfer and B. Krauskopf, “The ECM-backbone of the Lang-Kobayashi equations: A geometric picture,” Int. J. Bifur. Chaos, vol. 17 (2007), 1–14.
13. G. H. M. van Tartwijk, A. M. Levine, and D. Lenstra, “Sisyphus effect in semiconductor lasers with optical feedback,” IEEE J. Sel. Topics Quantum Electron., vol. 1 (1995), 466–472.
14. R. Vicente, S. Tang, J. Mulet, C. R. Mirasso, and J.-M. Liu, “Dynamics of semiconductor lasers with bidirectional optoelectronic coupling: Stability, route to chaos, and entrainment,” Phys. Rev. E, vol. 70, (2004), 0462161–11.

15. S. Newhouse, D. Ruelle, and F. Takens, “Occurrence of strange AxiomA attractors near quasi periodic flows on Tm, m _ 3,” Commun. Math. Phys., vol. 64 (1978), 35–40,.

16. J. Revuelta, C. R. Mirasso, P. Colet, and L. Pesquera, “Criteria for synchronization of coupled chaotic external-cavity semiconductor lasers,” IEEE Photon. Technol. Lett., vol. 14 (2002), 140–142.

17. A. Pikovsky, M. Rosenblum, and J. Kurths, Synchronization: A Universal Concept in Nonlinear Sciences, Cambridge, U.K.: Cambridge Univ. Press, 2001.

Chapter 5. General conclusion and outlook

"The most beautiful thing we can experience is the mysterious. It is the source of all true art and science."

Hermann Haken

5.1. Abstract

In this last chapter, we present the general conclusions of our research. We present the main contributions of the project to the field of semiconductor lasers coupled in different configurations. Finally, we outline some of the challenges to overcome in the future.

5.2. General conclusions

In this thesis, we have investigated and analyzed several aspects of optical injection induced different dynamics of semiconductor lasers when they are coupled in different configurations. The work was initially motivated by the willing to know the role of a coupling strength as a parameter in different configurations of coupled semiconductor lasers and the synchronization properties of this two coupled systems. Two different schemes were studied: two mutually-coupled semiconductor lasers and three semiconductor lasers arranged in an unidirectional ring. The advantages of each configuration were outlined in chapter 3 and 4. We recall here some of the interesting dynamics displayed by these two configurations.

The first objective (chapter 3) of this thesis was experimentally study the intensity dynamics and the optical spectra of two mutually delay-coupled semiconductor lasers respect to the two relevant parameters of the coupled system, namely the bias currents and the coupling strength of the lasers. The second objective (chapter 4) was to study a ring of three unidirectionally-coupled semiconductor lasers with respect to the coupling strength and see what route to chaos will exhibit in the semiconductor lasers and what synchronization is presented in this configuration with this parameter of control.

To obtain the aim of this thesis we realized an exhaustive revision of literature relate with different configurations of coupled systems of semiconductor lasers. With this study, we will provide a new step towards understanding of the behavior of coupled semiconductor lasers to select adequate laser parameters and configuration for optimal network performance.

We determined that semiconductor lasers subject to delayed optical injection in different configurations are desirable because of their potential applications in different areas, such as in optical secure communication, random number generation, and information processing, etc.

The results presented in this thesis are based on experimental and theoretical analyses of appropriate model (Lang-Kobayashi equations). Special attention has been given to the experimental characterization of the synchronization of two mutually-coupled semiconductor lasers for two different values of current of operation. Finally, for the configuration of three semiconductor lasers in a ring we found new results due to in previous studies, only a fixed value of the coupling strength was explored.

We have presented experimental and numerical studies for this two-coupled system from which we highlight the following points:

Highlights for two mutually delay-coupled semiconductor lasers:

- We have experimentally investigated the spectral and temporal characteristics of two mutually delay-coupled semiconductor lasers. By exploring the coupling strength dependence for two different values of the bias current, close to the laser threshold and well above it.

- We have found different dynamical regimes and different synchronization states. For low injection current ($I=1.02I_{th}$), we observed that the maxima of the cross-correlation function increased with decreasing attenuation between the lasers.

- For low injection current and low attenuation (strong coupling), we found the coexistence of low frequency fluctuations and continuous wave regimes; these two regimes alternated in time due to spontaneous emission and carrier noise.

- For low injection current and low attenuation, we found that the coupled lasers exhibited stable emission, their optical spectra were different from those of the solitary lasers; the central frequency of the coupled lasers was shifted towards lower frequencies, corresponding to the stable high gain compound cavity modes.

- We found that the average power of the lasers increased as the attenuation was decreased, independently of the changes in the dynamical regime.

- We found that the dynamics were more complex when the lasers were operated at $I=1.25I_{th}$.

- For current at $I=1.25I_{th}$, we found that the transition to chaotic emission with multiple compound cavity modes and a significant linewidth broadening were observed when the attenuation was decreased.

- For current $I=1.25I_{th}$, we have different synchronization states were identified for different attenuation values. Interestingly, the maximum cross-correlation between

the laser intensities changed non-monotonously as the attenuation factor was decreased. The qualitative changes in this dependence were associated with changes in the dynamical regimes. Correlation degraded in the strong chaos dynamical regime, while the maximum correlation was larger in the weak chaos regions.

- For current $I=1.25I_{th}$, and for smaller attenuations, the lasers were continuously synchronized but, due to the increasing complexity of the coupled system they lost synchronization.

- For current $I=1.25I_{th}$, and for strong coupling (very low attenuation, 0 dB to -12 dB) they synchronized in the generalized achronal synchronization state.

- Unlike the case of low bias current, for higher bias current, we did not observe bistability between chaotic pulsations and CW emission. It is worth highlighting that the generalized achronal synchronization state is particularly interesting because it originates from the bidirectional coupling of perfectly symmetric systems.

Highlights for two mutually delay-coupled semiconductor lasers:

- The numerical analysis performed provides a first understanding of the route that semiconductor lasers will exhibit for the coupling strength that is our parameter of control.

- In particular, we have found that the configuration of a three laser coupled in a ring scheme exhibit a quasiperiodic route to chaos as the coupling strength is increased.

- We have investigated the synchronization scenario that occurs upon the increase of the coupling strength. We identified different synchronization states of the semiconductor lasers. We found that in the periodic and quasiperiodic regimes the lasers are completely synchronized (when the delay time is compensated), in the chaotic state they lose synchronization, and as the coupling is further increased, the

lasers first become synchronized in phase and then almost synchronized. Although an increase in the coupling improves correlation, complete synchronization is never achieved even for 100% coupling.

- We analyzed our system using a fixed point analysis; for that we developed the Lang-Kobayashi equations and we assume that all lasers are identical therefore their amplitudes of the electric fields are equal. With this assumption we obtained a pair of transcendental equations, where their intersection defined a set of fixed points for a given effective coupling strength and phase. We found from zero coupling strength, exist only one stable fixed point, and the number of fixed points increases in pairs when the coupling strength is increased, and each pair is created in a saddle-node bifurcation.

- We obtained their chaotic trajectory projection of each laser.

- We did a bifurcation diagram where we can demonstrate the route to chaos via quasiperiodicity. We found that only two bifurcations are percussive to chaos, one standard Hopf bifurcation (HB) and one subsequent bifurcation to a two-frequency torus. When the third frequency is about to appear, a strange attractor simultaneously arises, since a three-frequency flow is destroyed by small perturbations. By means of three HBs, regular motion becomes highly unstable and is replaced by chaos.

5.3. Outlook

In the field of semiconductor lasers coupled, there is much work to do and many challenges ahead.

We will do an experimental observation of optical bistability of two bidirectional coupled identical semiconductor lasers and their numerical simulations based on Lang-Kobayashi model to show compare the agreement with our experimental observations. We will analyze the effect of coupling strength on the behavior of the lasers when we

are close to the current of threshold. We believe that optical bistability in mutually coupled semiconductor lasers can significantly advance the prospect of optical communication networks, in memory elements and all-optical signal processing and logic operation.

In addition, we will numerically and experimental study the possibility of encoding a message using as a carrier the chaotic output of one of the two semiconductor lasers in the configurations of mutually coupled SLs. A message will be encoded by a time dependent attenuation of the carrier. Then the encoded message will be recovered by operating over both the input and output of the receiver.

Finally, we analyze theoretical the evidence of the emergence of bistability in two bidirectionally-coupled semiconductor lasers and prove that we have the same results in theory and experimental setup. We will try to present a mechanism in which noise intrinsic to a semiconductor laser stabilizes a deterministically unstable steady state.

Appendix A. List of instruments and components

In this appendix we present the detailed references to the components and instruments used in the experiments:

1. Eblana EP1550-DM-BAK-001: DMLD
2. Thorlabs LM14S2: Buttery mount
3. Thorlabs PRO8000: LD controller
4. Absys C-WD-AL-50-H-2210-35-AP/AP: Fiber coupler (50/50)
5. Absys PII-55-P-D-2-22-LL-1: Fiber isolator
6. Thorlabs FPC560: Fiber polarization controller
7. Thorlabs PM30: Optical powermeter
8. Anritsu MS9710C: Optical spectrum analyzer
9. Miteq DR-125G-A: Fast photodiodes
10. Anritsu MS2667C: Electrical spectrum analyzer
11. LeCroy SDA816Zi: High bandwidth oscilloscope

Appendix B. Publications

In this appendix we present the publications that we publish in index journals:

1. Diana A. Arroyo-Almanza, Alexander N. Pisarchik, and Flavio R. Ruiz-Oliveras, "Route to chaos in a ring of three unidirectionally-coupled semiconductor lasers," IEEE Photon. Technol. Lett., vol. 24 (2012), 605-607.

2. D. A. Arroyo-Almanza, A. N. Pisarchik, I. Fischer, C. R. Mirasso, and M. C. Soriano, "Spectral properties and synchronization scenarios of two mutually delay-coupled semiconductor lasers. Opt. Comm.," vol. 301-302 (2013), 67-73.

3. S. Heiligenthal, T. Jüngling, D. A. Arroyo-Almanza, O. D'Huys, M. C. Soriano, I. Fischer, I. Kanter, and W. Kinzel, "Strong and weak chaos in networks of semiconductor lasers with time-delayed couplings," arXiv:1210.1887